Agricultural and Forest Meteorology 358 (2024) 110215

Contents lists available at ScienceDirect

Agricultural and Forest Meteorology

journal homepage: www.elsevier.com/locate/agrformet

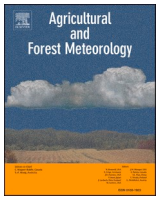

Hydrometeorology-wildfire relationship analysis based on a wildfire bivariate probabilistic framework in different ecoregions of the continental United States

Ke Shi [a,*], Yoshiya Touge [b], So Kazama [c]

[a] State Key Laboratory of Simulation and Regulation of Water Cycle in River Basin, China Institute of Water Resources and Hydropower Research, Beijing 100038, China
[b] Disaster Prevention Research Institute, Kyoto University, Uji, Kyoto, 611-0011, Japan
[c] Department of Civil and Environmental Engineering, Tohoku University, Sendai, Miyagi, 980-8579, Japan

ARTICLE INFO

Keywords:
Wildfire
Hydrometeorology
Wildfire regime
Copula

ABSTRACT

Wildfires are a natural part of the ecosystem in the U.S.. It is vital to classify wildfires using a comprehensive approach that simultaneously considers wildfire activity (the number of wildfires) and burned area. On this basis, the influence of hydrometeorological variables on wildfires can be further analyzed. Therefore, this study first classified wildfire types using a wildfire bivariate probability framework. Then, by considering six hydrometeorological variables, the dominant hydrometeorological variables for different wildfire types in 17 ecoregions of the United States were quantified. In addition, based on the results of this hydrometeorology-wildfire relationship analysis, we obtained new clusters that simultaneously considered wildfire characteristics and the impact of hydrometeorology on wildfires. In particular, the results were as follows: (1) Through the probability of wildfire bivariate statistical characteristics, wildfires could be classified into five types in this paper: WT-1 (mega-wildfire), WT-2 (joint wildfire-1), WT-3 (joint extremes), WT-4 (joint wildfire-2), and WT-5 (super frequent wildfires); (2) The dominant hydrometeorological variables under different wildfire types were discussed in 17 ecoregions of the United States; and (3) In the four new cluster regions, intensifying droughts are a concern in clusters 1 and 4, while there are multiple concerns in cluster 3, namely, stronger winds, higher temperatures, and more drought.

1. Introduction

Wildfires constitute an integral ecological process in the natural Earth system associated with regional and global biogeochemical cycles, human activities, and vegetation structure (Bowman et al., 2009). Additionally, the postfire effect on the physical properties of soil (e.g., infiltration rates (Robichaud, 2000), runoff and erosion response (Moody et al., 2013; Vieira et al., 2015)), and biological activity (Van Mantgem et al., 2020; Yelenik et al., 2013) changes with the characteristics of wildfire. Therefore, before discussing the postfire effect, a comprehensive perspective is essential to elucidate what kind of wildfire has a higher severity or a higher risk, especially in the United States, which hosts 823 million acres of forest and woodland areas (Oswalt et al., 2019). Over just a four-year period from 2017 to 2020, nearly 200 lives were lost, and more than 45,000 structures were destroyed in California wildfires (Swain, 2021). In particular, wildfires resulting in large burned areas have increased in the western United States in recent years (Dennison et al., 2014; Zhang et al., 2020). Subjectively, it appears that more wildfire activities could lead to more severe wildfires and larger burned areas. However, the reduction in wildfire activities (number of wildfires) driven by policy and wildfire management has resulted in changes in the vegetation structure and an increase in fuel accumulation in the western United States (Hurteau et al., 2014). As a consequence, wildfire suppression and the subsequent increase in fuel loads have coincided with warmer and drier wildfire seasons, causing high-severity wildfire events yielding large burned areas (Dennison et al., 2014; Fulé et al., 2003; Holden et al., 2018; Parks and Abatzoglou, 2020; Steel et al., 2015). These two seemingly contradictory situations are attributed to the unique structure of the relationship between the wildfire activity (the number of wildfires) and burned area, posing challenges to comprehensively assess the wildfire characteristics.

In particular, to describe the relationship among wildfire statistics in

* Corresponding author.
E-mail address: Ke.dlut@outlook.com (K. Shi).

https://doi.org/10.1016/j.agrformet.2024.110215
Received 8 August 2022; Received in revised form 26 July 2024; Accepted 3 September 2024
Available online 20 September 2024

detail, this study first provides a concept map of wildfire bivariate statistical characteristics, as shown in Fig. 1. In this wildfire bivariate statistical characteristics, two lines control the wildfire activity and burned area: the wildfire increase vector (WIV), and wildfire extent vector (WEV). Additionally, When the wildfire activity (or burned area) value is greater than 99% of the wildfire activity (or burned area) value in the sample, it will be considered extreme wildfires (wildfire extreme zone as shown in Fig. 1), and five different types of wildfires can be seen in the wildfire extreme zone. Among them, the most extensive attention is given to mega-wildfires (wildfire type-1, burned area value is greater than 99% of the burned area value in the sample), such as the 2014 California mega-wildfire in the United States (Coen et al., 2018), the 2017 mega-wildfire in Chile (Pliscoff et al., 2020) and the 2019/2020 mega-wildfire in Victoria, Australia (Geary et al., 2022). This kind of wildfire has nonnegligible negative social, economic, and environmental effects due to its large amount of burned area (Jones et al., 2021; Le Breton et al., 2022; Shen et al., 2022). On the other hand, studying super frequent wildfires (wildfire type-5, wildfire activity value is greater than 99% of the wildfire activity value in the sample) in different regions, such as Portugal (Moreira et al., 2010), Australia (Clarke et al., 2019), and the United States (Cattau et al., 2020), is also a hot topic in wildfire science. A related issue associated with super frequent wildfires is that they may result in alien species expansion (Syphard et al., 2009). For example, biodiversity in California is threatened by shrubbery conversion to alien annual grasses under the influence of super frequent wildfires (Keeley et al., 2005). However, the discussion of the other three types of wildfires (joint wildfire-1, joint extreme wildfire, joint wildfire-2) has thus far been very limited and lack corresponding definitions. This article defines these three types of wildfires for the first time and provides a detailed discussion. Accurate classification of various wildfire types, utilizing bivariate statistical characteristics, is essential for a comprehensive understanding of wildfire changes. This classification is particularly crucial when distinguishing between super frequent wildfires (classified as wildfire type-5) and mega-wildfires (classified as wildfire type-1). Without this nuanced characterization, it becomes challenging to analyze the potential mutual transformation between type-1 and type-5 wildfires, under varying weather conditions and human influences. A thorough understanding of these transformative changes, which represent a shift in the dominant wildfire types within a specific wildfire regime, is pivotal for the development and implementation of targeted wildfire prevention and control strategies. Thus, only by systematically understanding the relationship and causes of different types of wildfires using wildfire bivariate statistical characteristics can we implement more targeted wildfire prevention plans, thereby increasing the resilience of vegetation and reducing the losses caused by wildfires.

Existing studies have extensively explored the relationship between hydrometeorological variables and burned area or wildfire activity from

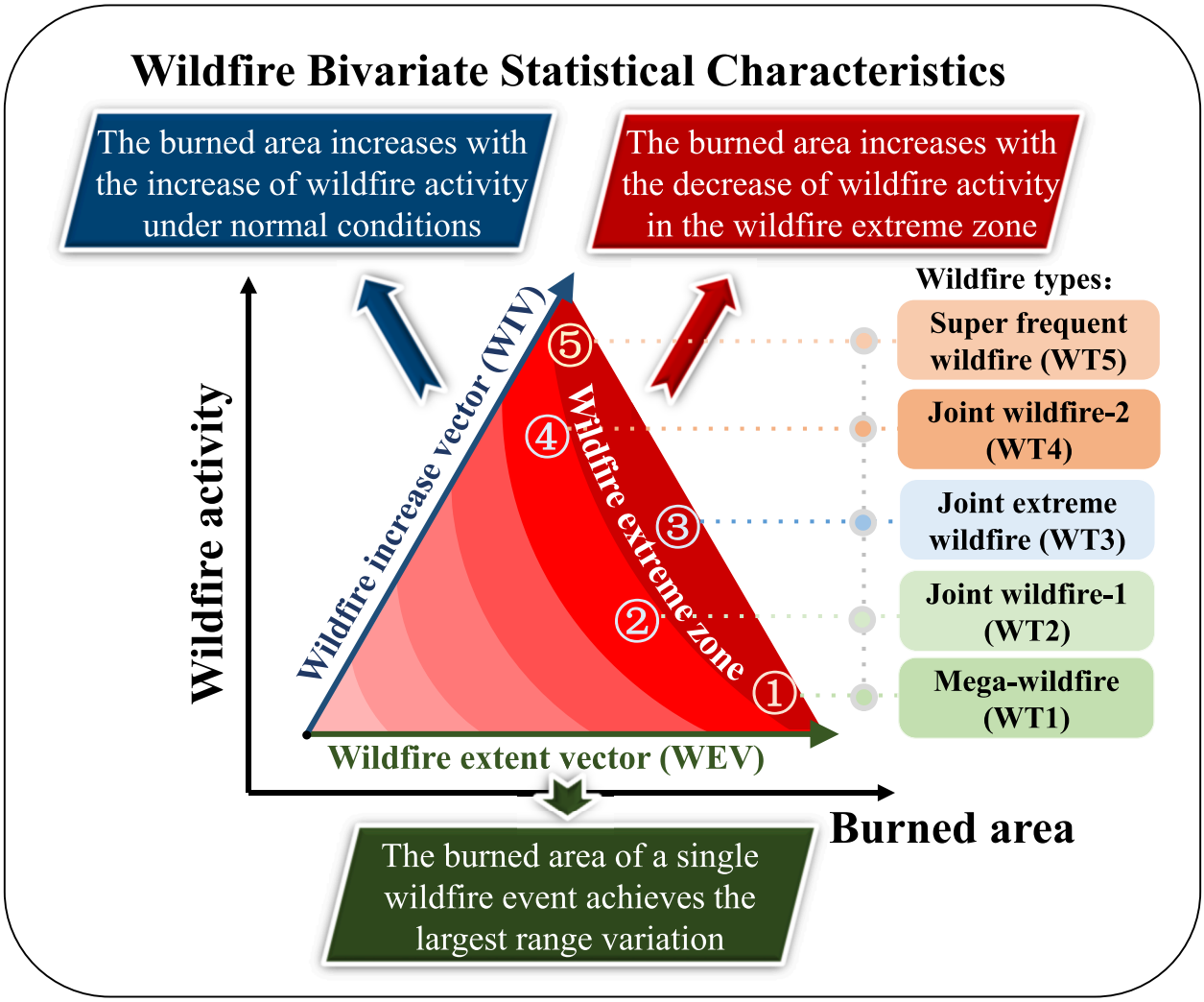

Fig. 1. Conceptual diagram of the wildfire bivariate statistical characteristics and the locations of five typical wildfire types. The wildfire extreme zone includes wildfire types 1–5, indicating extreme wildfire conditions.

a univariate wildfire perspective. Antecedent hydrometeorological conditions, such as reduced precipitation, high temperature, and drought events, are found to influence these wildfire events through the preconditioning of fuels (Littell et al., 2016). In contrast, wind speed can play only a secondary role in wildfire activity (de Dios et al., 2022) but it is more sensitive to the burned area (Shabbir et al., 2020). Wind speed is a key factor affecting the spread of wildfire after the wildfire has begun (Andrews et al., 2013; Özbayoğlu and Bozer, 2012). Once a wildfire occurs, the severity of the wind will affect the ultimate size of the wildfire event (Keeley and Syphard, 2017). High temperatures can increase evaporation, resulting in drier fuels and water loss in forest flora, thus increasing wildfire activity (Mansoor et al., 2022). The largest wildfire-burned area was found to be associated with high-temperature events (Aldersley et al., 2011; Cardil et al., 2015; Wang et al., 2021). Moreover, long-term trends in the burned area and wildfire activity are more significantly affected by precipitation and drought than short-term trends (Andela et al., 2017; Flannigan et al., 2016; Wei et al., 2020). To date, several different types of drought indices, such as the Standardized Precipitation-Evapotranspiration index (SPEI) (Cardil et al., 2019; Rodrigues et al., 2021), Palmer Drought Severity Index (PDSI) (Collins et al., 2006; Flatley et al., 2011) and surface soil moisture (SSM) (Bartsch et al., 2009; Dadap et al., 2019), have been used in the discussion of the relationship between drought and wildfire. The regional depletion of soil (e.g., PDSI and SSM) and atmospheric (e.g., SPI) moisture can lead to a low moisture content in duff (both fibrous and humic horizons) and surface fuels and can ultimately result in a higher potential for widespread wildfires (Littell et al., 2016). Drought affects the likelihood of ignition at multiple time scales, affecting fuel moisture and propagation on shorter time scales and affecting fuel availability by controlling ecosystem characteristics and productivity on longer time scales (Loehman et al., 2014). Considering wildfire activity and burned area separately, the relationship between hydrometeorological variables and wildfire activity or burned area is well documented. In contrast, the relationship between meteorological variables and wildfire bivariate statistical characteristics is still emerging. In particular, the effect of meteorological conditions on the simultaneous occurrence of extreme burned area and extreme wildfire activity, i.e., wildfire type-2 (WT2), -3 (WT3), and -4 (WT4), has not been explored. Also, it is difficult to fairly compare burned area and wildfire activity in previous studies because of the large magnitude differences between them. Using a probabilistic framework makes it possible to compare WT1 and WT5 at the same extreme level.

In the United States, since 2000, an average of 70,072 wildfires have occurred each year, burning over 2.8 million ha annually (Hoover and Hanson, 2021). Moreover, wildfires in the United States are becoming increasingly frequent, leading to greater environmental degradation, property damage, and economic loss (Dennison et al., 2014). Wildfires in the United States are projected to cost nearly $1.8 billion per year in wildfire suppression by 2025 (USFS, 2015). The United States experienced not only multiple mega-wildfire events (Buckland, 2019), such as the 2002 Biscuit wildfire (Harma and Morrison, 2003), the 2013 Rim wildfire (Povak et al., 2020), the 2007 Zaca wildfire (Keeley et al., 2009), and the 2014 King wildfire (Coen et al., 2018), but also super frequent wildfire events (Cattau et al., 2020). Additionally, considering geology, landforms, soils, vegetation, climate, land use, wildlife, and hydrology, the United States can be divided into different ecoregions (Omernik and Griffith, 2014), and wildfires in different ecoregions show spatial heterogeneity. For example, the average burned area in the western United States was more extensive than that in the eastern United States (Nagy et al., 2018). Additionally, wildfire activity showed a decreasing trend in Mediterranean California but an increasing trend in the Rocky Mountains (Dennison et al., 2014). Even in the same regions, wildfire characteristics can show temporal heterogeneity under the current anthropogenic climate change. As the climate becomes warmer and drier, the shift in vegetation from mesic forest and cold forest to dry forest and then to shrubland/grassland becomes possible, corresponding to an increasing trend of wildfire activity at first, followed by a decreasing trend (Parks et al., 2018). The wide variety of wildfires and spatiotemporal heterogeneity of wildfire characteristics make the United States a suitable study area for examining the hydrometeorology-wildfire relationship.

Based on the wildfire bivariate statistical characteristics, we examined the potential relationships among hydrometeorological variables and wildfires from a bivariate perspective. In addition, most studies of hydrometeorology in relation to wildfires have examined the relationship between seasonal or annual hydrometeorological variables and wildfire variables (wildfire activity and burned area) to measure and link patterns of the key drivers of wildfires (Higuera and Abatzoglou, 2021; Holden et al., 2018; van Wagtendonk et al., 2020). Nevertheless, the relationship between hydrometeorology and wildfire should be examined on at least a monthly scale to prevent extreme weather conditions from being overlooked due to averaging. In particular, we addressed the following key issues in hydrometeorology-wildfire relationships: (1) the dominant hydrometeorological variables of the five types of wildfires, (2) the possible intrinsic relationship between the five types of wildfires, and (3) the significant changes in hydrometeorological variables that need to be noted in the new, different wildfire clusters.

2. Materials

2.1. Wildfire data

In this study, the United States, which has many wildfire events, was chosen as the study area. This paper divides the United States into 17 ecoregions based on Environmental Protection Agency regional offices (McMahon et al., 2001; Omernik, 1987, 2004; Omernik and Griffith, 2014), as shown in Fig. 2. Wildfire statistics data in the United States were obtained from the 5th Edition of the Forest Service Fire Program Analysis - Fire Occurrence Database (FPA-FOD) (Short, 2021). This comprehensive dataset includes 2.17 million georeferenced wildfire records, representing a total burned area of 667.7 billion m^2 from 1992 to 2018. These wildfire records were acquired from the reporting systems of federal, state, and local fire organizations. For original geographic reference wildfire records, due to the lack of information, the dataset can only provide the coordinates of the starting point and the final burned area, and cannot provide the shape of the combustion, which is simplified into a fire point with an area. Spatially, we have adopted a higher resolution ($0.5^\circ \times 0.5^\circ$) to minimize the need for cross-grid wildfire statistics. For wildfire events that exceed the grid, we will count them at the starting grid of the wildfire occurrence, and do not repeat the statistics for the grids that cross later. To construct the monthly time series, each wildfire event was plotted in grid cells of specific months according to its discovery date and end date. For wildfires that continue to burn across months, the wildfire activity will be counted in the starting month based on the start date of the wildfire, and will not be counted in the month when the wildfire ends. Grid cells with fewer than 100 wildfire records during the 27 years were removed to ensure accurate estimation of the univariate distribution and bivariate distribution, as shown in Fig. 3. This approach may overlook areas with fewer wildfire events, but this article will focus more on understanding the causes of wildfires in wildfire-prone areas. Additionally, log transformation was subsequently performed to process the wildfire statistics into log-burned area (LBA) and log-wildfire activity (LFA). Log transformation is commonly used in the statistical analysis of wildfires and can highlight wildfire-sensitive ecosystems that are rarely affected but have a lower vegetation restoration capability than other wildfire-dependent ecosystems. To avoid a 0 value after log transformation, months with only one wildfire event were converted to 0.1 in this study.

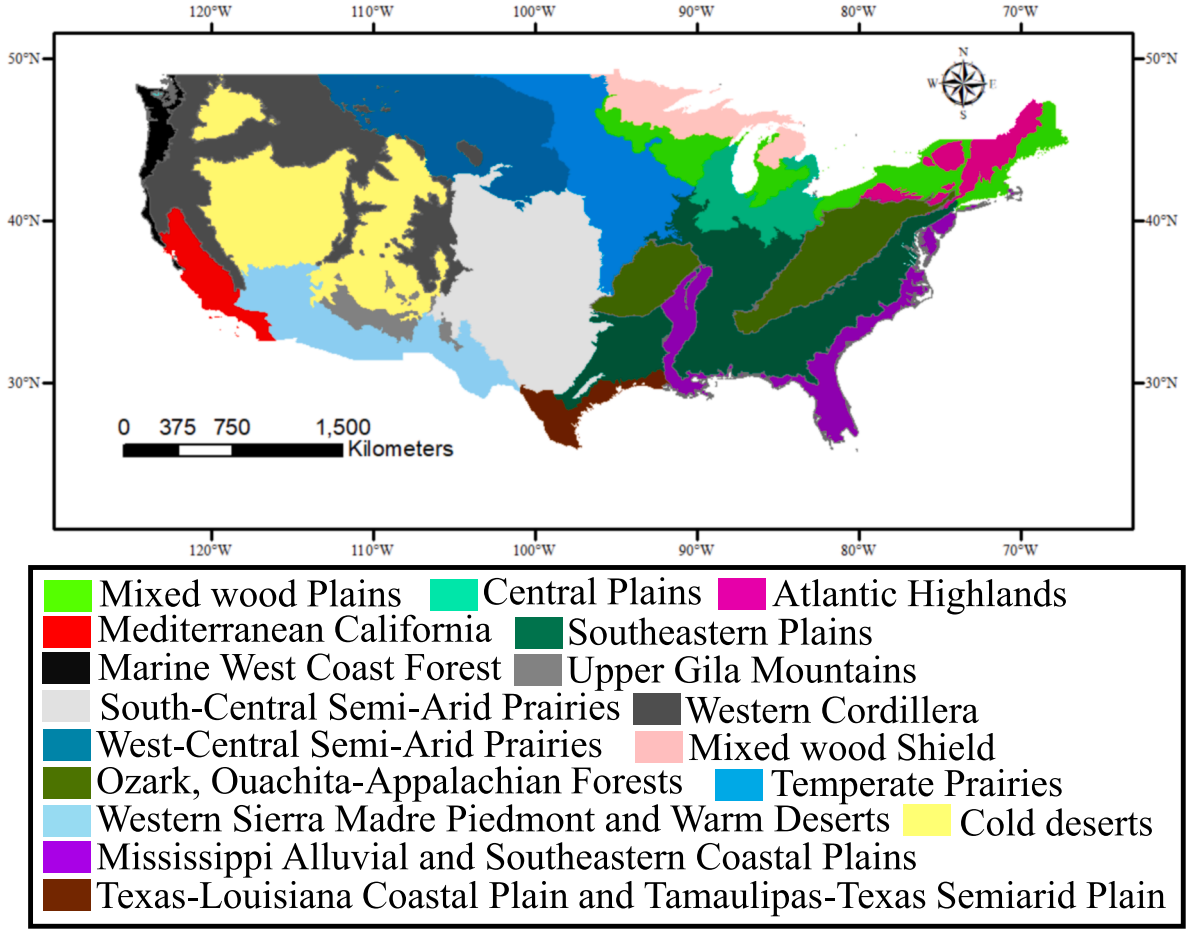

Fig. 2. Ecoregions of the contiguous United States.

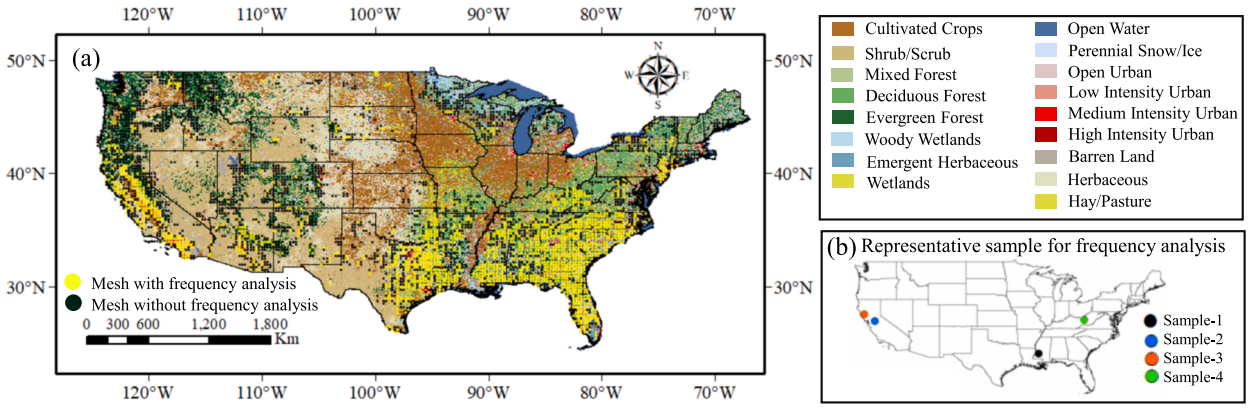

Fig. 3. Distribution of vegetation in the contiguous United States and the reserved grid cells in this study. Figure 3(b) shows the location of the representative sample considered in the frequency analysis. The land cover data in the figure comes from National Land Cover Database 2021.

2.2. Basic meteorological data

The underlying meteorological data for this study were obtained from ERA5 hourly data at a 0.5° × 0.5° resolution from 1992 to 2018 (Hersbach et al., 2018). The variables that were directly used to analyze the relationship between hydrometeorological variables and wildfire were temperature (TEM), wind speed (WS), and precipitation (PRE). Hourly TEM and WS data were calculated as monthly averages, and hourly PRE data were aggregated to monthly totals. Other hydrometeorological data, such as dewpoint temperature, barometric pressure, shortwave radiation, and longwave radiation, were used in the calculation of the drought index.

2.3. Calculated drought index

In this study, three calculated drought indices were applied: the SPEI, PDSI, and SSM.

(I) In particular, the PDSI (Palmer, 1965) is calculated from the monthly moisture anomalies (MMA) determined by estimating

the difference between the actual precipitation and the precipitation required for the climate to be suitable for existing conditions (Zhai et al., 2010). The formula used to calculate the MMA is shown in Eq. (1). The PDSI incorporates antecedent precipitation, water supply, and water demand into a hydrological system (Dai et al., 2004).

$$MMA_i = K(PRE - (\alpha_i PET + \beta_i PR + \varphi_i PRO - \delta_i PL)) \quad (1)$$

The MMA can be used to show the dryness/wetness in month *i*. *PRE, PET, PR, PRO,* and *PL* represent precipitation, potential evapotranspiration, potential recharge, potential runoff, and potential loss, respectively. For a more detailed description of the parameters, please refer to Wells et al. (2004). The four potential values are adjusted based on the climate of the region using α_i, β_i, φ_i, and δ_i, leading to the climatically appropriate for existing conditions (CAFEC) potential values. These weighting factors, known as water-balance coefficients, are determined as follows:

$$\alpha_i = \frac{\overline{ET}}{\overline{PET}} \quad (2)$$

$$\beta_i = \frac{\overline{R}}{\overline{PR}} \quad (3)$$

$$\varphi_i = \frac{\overline{RO}}{\overline{PRO}} \quad (4)$$

$$\delta_i = \frac{\overline{L}}{\overline{PL}} \quad (5)$$

where i ranges over the months of the year. The bar over a term indicates an average value.

As for the K, it is actually a refinement of K', which is Palmer's general approximation for the climate characteristic of a location. Palmer (1965) derived the equations for K' and for K, respectively, where MMA_i is the average moisture departure for the appropriate month:

$$K_i' = 1.5\log_{10}\left(\frac{\frac{\overline{PE_i}+\overline{R_i}+\overline{RO_i}}{\overline{P_i}+\overline{L_i}} + 2.8}{\overline{MMA_i}}\right) + 0.5 \quad (6)$$

$$K_i = \frac{17.67}{\sum_{j=1}^{12}\overline{D_j}K_j'}K_i' \quad (7)$$

Through the MMA, the PDSI value can be calculated for a given month using the following formula:

$$PDSI_i = \begin{cases} \dfrac{MMA_i}{3}, i = 1 \\ PDSI_{i-1} + \dfrac{MMA_i}{3} - 0.103PDSI_{i-1}, i > 1 \end{cases} \quad (8)$$

In particular, the PET was calculated through the Penman–Monteith equation rather than the Thornthwaite equation because the former can more realistically estimate potential evapotranspiration. The specific formula is listed as follows:

$$PET = \frac{0.408\Delta\,(R_n - G) + \gamma\frac{900}{T+273}U_2\,(e_s - e_a)}{\Delta\ + \gamma\,(1 + 0.34U_2)} \quad (9)$$

where R_n is the net radiation, G is the soil heat flux density, T is the air temperature at a 2 m height, U_2 is the wind speed at a 2 m height, e_s is the vapor pressure of the air at saturation, e_a is the actual vapor pressure, Δ is the slope of the vapor pressure curve and γ is the psychrometric constant (Allen et al., 1998).

(II) The SPEI is based on the monthly difference between the *PRE* and *PET* at different time scales of interest. The SPEI at different time scales can represent different climatic water balances. With a value for *PET*, the difference between the *PRE* and *PET* for month *i* can be calculated as follows:

$$D_i = PRE_i - PET_i \quad (10)$$

The calculated D_i values are aggregated at different time scales. The difference in a given month j and year i depends on the chosen timescale k. For example, the accumulated difference for one month in a particular year i with a 12-month timescale can be calculated as follows (Vicente-Serrano et al., 2010):

$$X_{i,j}^k = \begin{cases} \sum_{l=13-k+j}^{12} D_{i-1,l} + \sum_{l=1}^{j} D_{i,l}, j < k \\ \sum_{l=j-k}^{j} D_{i,l}, j \geq k \end{cases} \quad (11)$$

where $D_{i,\ l}$ is the P − PET difference in month l of the year i.

Based on its behavior at the most extreme values, the log-logistic distribution is very well adapted to standardizing the D series to obtain the SPEI (Vicente-Serrano et al., 2010). The probability density function of a three-parameter log-logistic distributed variable is expressed as:

$$f(x) = \frac{\beta}{\alpha}\left(\frac{x-\gamma}{\alpha}\right)^{\beta-1}\left[1 + \left(\frac{x-\gamma}{\alpha}\right)^{\beta}\right]^{-2} \quad (12)$$

where α, β, and γ are the scale, shape, and origin parameters, respectively, for D values in the range ($\gamma > D < \infty$).

According to Ahmad et al. (Vicente-Serrano et al., 2010), the l-moment procedure is the most robust and easy approach to estimating the parameters of the log-logistic distribution. When l-moments are calculated, the parameters of the Pearson III distribution can be obtained following the methods of Singh et al. (Singh et al., 1993).

$$\beta = \frac{2w_1 - w_0}{6w_1 - w_0 - 6w_2} \quad (13)$$

$$\alpha = \frac{(w_0 - 2w_1)\beta}{\Gamma\left(1 + \frac{1}{\beta}\right)\Gamma\left(1 - \frac{1}{\beta}\right)} \quad (14)$$

$$\gamma = w_0 - \alpha\Gamma\left(1 + \frac{1}{\beta}\right)\Gamma\left(1 - \frac{1}{\beta}\right) \quad (15)$$

The w_i is the probability-weighted moments (PWMs), and PWMs of order i are calculated as:

$$w_i = \frac{1}{N}\sum_{j=1}^{N}(1 - F_j)^i D_i \quad (16)$$

$$F_j = \frac{j - 0.35}{N} \quad (17)$$

where F_j is a frequency estimator calculated by Hosking (1990).

The cumulative distribution function of the D series, according to the log-logistic distribution, is as follows:

$$F(x) = \left[1 + \left(\frac{\alpha}{x-\gamma}\right)^{\beta}\right]^{-1} \quad (18)$$

The SPEI can be easily obtained as the standardized values of $F(x)$ (Abramowitz and Stegun, 1964):

$$SPEI = W - \frac{C_0 + C_1 W + C_2 W^2}{1 + d_1 W + d_2 W^2 + d_3 W^3} \quad (19)$$

where:

$$W = \sqrt{2 - \ln(P)}, P \leqslant 0.5 \quad (20)$$

and P is the probability of exceeding a determined D value, $P = 1 - F(x)$. If $P > 0.5$, then P is replaced by $1 - P$, and the sign of the resultant SPEI is reversed. The constants are C_0=2.515517, C_1=0.802853, C_2=0.010328, d_1=1.432788, d_2=0.189269, and d_3=0.001308.

An SPEI of one month usually represents the meteorological drought, while a timescale of 3–6 months is considered an agricultural drought index. Longer scales, such as 6 months and 12 months, are used to indicate hydrological drought and to monitor surface water resources (Beguería et al., 2014; Hayes et al., 2011). It should be noted that the SPEI used in this study is the mean of SPEI1, SPEI3, SPEI6, SPEI9, and SPEI12.

(III) Unlike the common drought indices that use only precipitation or limited meteorological elements in their calculations, SSM is affected by numerous factors, such as topography, soil type, and multiple meteorological elements. Additionally, soil moisture, as a good drought index, can reflect recent precipitation and antecedent conditions, indicating the vegetation potential and available water storage (Keyantash and Dracup, 2002). The soil moisture data used in this study were derived from simulations using the Simple Biosphere including the Urban Canopy (SiBUC) model developed by Tanaka (Tanaka, 2005), which was developed based on the Simple Biosphere Model (SiB) (Sellers et al., 1996). In addition, a single-layer snow model was also considered in the SiBUC model, providing an opportunity to consider the water supply in spring based on the snow melting process. This model has been utilized for not only regional-scale analyses but also for global-scale analyses, such as in Turkey (Fujihara et al., 2008), Japan (Kotsuki et al., 2015), and Southeast Asia (Kotsuki and Tanaka, 2013b). Through validation with the measured SSM, the SSM simulated by the SiBUC had good accuracy (Shi et al., 2022). And some studies have found that SiBUC can reproduce annual river discharge well in this basin when accurate precipitation records are used (Kotsuki and Tanaka, 2013a, 2013b). The SiBUC is a model based on physical processes, which is more credible than the empirical model. Notably, the soil moisture simulated by the SiBUC in this study is the saturation ratio in the first layer. In the calculation of the SiBUC, the effects of human activities were eliminated by removing irrigation. After obtaining the daily soil moisture, the monthly minimum soil moisture was extracted to show the driest situation every month.

In addition to hydrometeorological data, the land use and land type data were obtained from the Global Land Cover Characterization (Loveland et al., 2000). The soil parameters and vegetation parameters such as the leaf area index were obtained from ECOCLIMAP (Champeaux et al., 2005).

3. Methodology

Here, we analyzed hydrometeorology-wildfire relationships for 324 months of wildfire data from 1992 to 2018 to assess how these relationships persist across different ecoregions of the United States. Specifically, the bivariate probability of wildfire was first calculated from the joint probability distribution. The five different types of wildfires were classified according to their probability threshold. Then, the probability of hydrometeorological variables corresponding to the different wildfire types was calculated to further discuss the relationship between hydrometeorology and wildfire. Based on our hydrometeorology-wildfire relationship results, we additionally performed a cluster analysis to obtain new wildfire clusters with similar wildfire characteristics and hydrometeorological impacts on the wildfire. Finally, the trends of each hydrometeorological variable within the new wildfire clusters were analyzed.

The flowchart of the calculation is shown in Fig. 4. Specifically, methods 3.1 to 3.2 were used to calculate the frequency of hydrometeorological elements and the wildfire priority index, respectively. The calculation results of the wildfire priority index correspond to Chapter 4.1. The wildfire priority index was used to classify wildfire types, corresponding to result 4.2. The frequency of extracting hydrological and meteorological elements under different types of wildfires ranged from 4.3 to 4.4 in the results. Using the result of 4.4 as input, the clustering method of 3.4 was used to obtain the homogeneous zone of wildfire in 4.5, and the trend analysis method of 3.5 was used to calculate the changing trend of wildfire causes in 4.6.

3.1. Optimal selection of univariate distribution

The l-moment has been widely established in statistics for determining theoretical probability distributions (Bhatti et al., 2019; Guttman et al., 1993; Ye et al., 2018). The l-moment is less affected by sampling variability, which is more robust to outliers in the data (Guttman et al., 1993). The three important parameters τ_2 (L-CV), τ_3 (L-skewness), and τ_4 (L-kurtosis) included in l-moment can be used to calculate a variety of different distribution functions (Hosking, 1990), including one-parameter, two-parameter, three-parameter, and four-parameter distribution functions. A total of seven commonly considered marginal distributions were selected in this research. The specific expressions of these functions and the parameter estimates are provided in Table 1. Specifically, for a time series $X(i)$ of length n, the samples are first sorted in ascending order: $X(1) \leq X(2) \leq \ldots \leq X(n)$. Then, the linear combination of probability weighted moments is given in Eq. (21) (Greenwood et al., 1979):

$$\beta_0 = \frac{1}{n}\sum_{i=1}^{n} X(i)\beta_1 = \sum_{i=1}^{n-1}\left[\frac{n-i}{n(n-1)}\right]X(i)\beta_3 = \sum_{i=1}^{n-2}\left[\frac{(n-i)(n-i-1)}{n(n-1)(n-2)}\right]X(i) \quad (21)$$

The first three l-moments for the population can be calculated by Eq. (22):

$$\lambda_1 = \beta_0,\ \lambda_2 = 2\beta_1 - \beta_0,\ \lambda_3 = 6\beta_2 - 6\beta_1 + \beta_0 \quad (22)$$

where λ_1, λ_2, and λ_3 correspond to the position, scale, and shape moments, respectively. Then, the l-moment ratios are calculated as follows:

$$\tau_2 = \frac{\lambda_2}{\lambda_1},\ \tau_3 = \frac{\lambda_3}{\lambda_2},\ \tau_4 = \frac{\lambda_4}{\lambda_2} \quad (23)$$

Through the above l-moment ratios, distribution parameters can be calculated, as shown in Table 1. For more details, please refer to Hosking (Hosking, 1990; Hosking and Wallis, 1997). A total of seven commonly used marginal distributions were selected in this research, and the expressions of specific functions are shown in Appendix 1 (Table A1).

For the goodness of fit, the probability plot correlation coefficient (PPCC) and the root mean square error (RMSE) are utilized. The RMSE is one of the most widely used indicators for goodness of fit (Xu et al., 2015; Yang et al., 2018). The specific calculation functions are shown in Functions 24–25. Similarly, the PPCC judges how well the simulated l-skewness and l-kurtosis of a fitted distribution match the average regional l-skewness and l-kurtosis values obtained from the observed data. The PPCC statistic has a maximum value of 1. The PPCC has been shown to be a powerful statistic for evaluating the goodness of fit of a wide range of alternative distributional hypotheses (Stedinger, 1993) and for performing hypothesis tests of various two-parameter distributional alternatives. The specific calculation process of PPCC can be

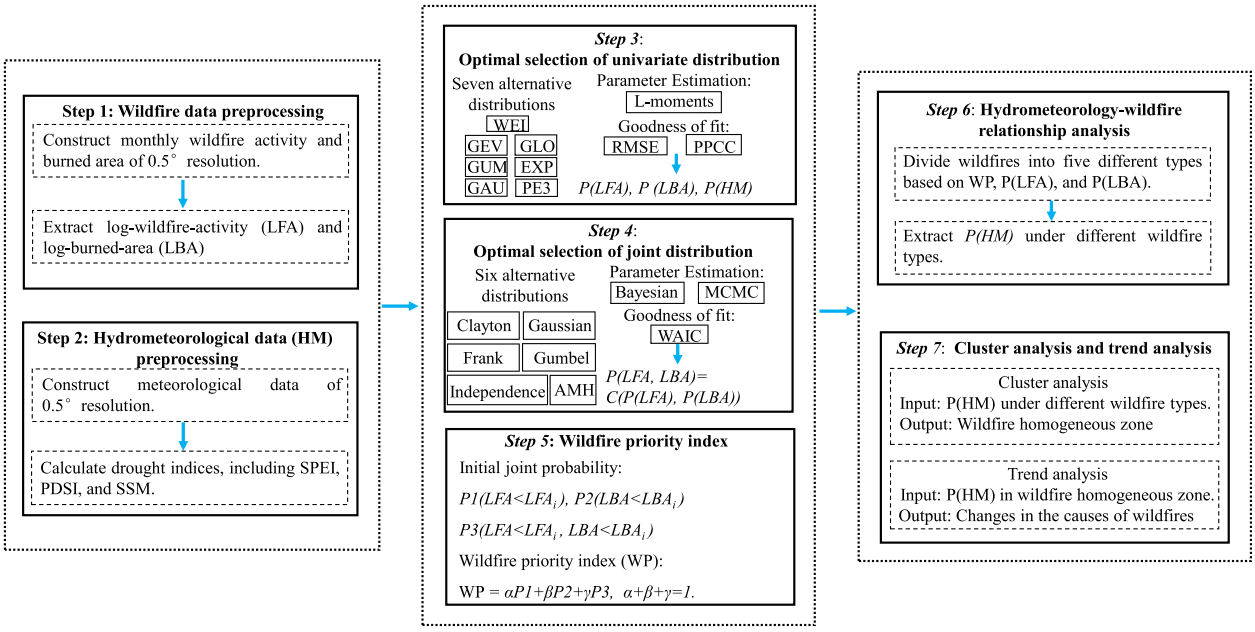

Fig. 4. The flowchart of calculation. LFA: log wildfire activity, LBA: log burned area, HM: hydrometeorological elements.

Table 1
Trend categories according to the Z values.

Categories	Z values
Significant increasing trend	[1.96, +∞)
Weak increasing trend	[1.64, 1.96)
No significant increasing trend	[0, 1.64)
No significant decreasing trend	(−1.64, 0)
Weak decreasing trend	(−1.96, −1.64]
Significant decreasing trend	(-∞, −1.96]

found in Function 26.

$$Pe = P(A \leqslant a_i) = \frac{\sum_{m=1}^{i} N_m - 0.44}{n + 0.12} \tag{24}$$

$$RMSE = \sqrt{\frac{1}{n-1}\sum_{i=1}^{n}(P_e - P_t)^2} \tag{25}$$

Where P_e and P_t are empirical cumulative probability and theoretical cumulative probability, respectively.

$$PPCC = \frac{\sum_{i=1}^{n}(X_i - \overline{X})(M_i - \overline{M})}{\sqrt{\sum_{i=1}^{n}(X_i - \overline{X})^2 (M_i - \overline{M})^2}} \tag{26}$$

Where X_i and M_i are the ordered observations and the order statistic medians, respectively; $\overline{X}$ and $\overline{M}$ are the average value of observations and statistic medians, respectively (Filliben, 1975).

3.2. Optimal selection of joint distribution

The parameter estimation approach of the bivariate distribution is Bayesian analysis and the Markov chain Monte Carlo (MCMC) algorithm. Bayes' law conveniently attributes all the modeling uncertainties to the parameters and estimates the posterior distribution of the model parameters as follows:

$$p(\theta|\widetilde{Y}) = \frac{p(\theta)p(\widetilde{Y}|\theta)}{p(\widetilde{Y})} \tag{27}$$

in which $P(\theta)$ and $P(\theta|\widetilde{Y})$ signify the prior and posterior distributions of the parameters, respectively. Empirically-based constants in each model can be simply removed from the analysis if the main goal is to estimate the posterior distribution of the parameters and posterior parameter distributions can be estimated as follows:

$$P(\theta|\widetilde{Y}) \propto P(\theta)P(\widetilde{Y}|\theta) \tag{28}$$

Bayes' Eq. (27) is usually difficult to calculate. To analytically and numerically solve this problem, MCMC is adopted to sample from the posterior distribution. MCMC algorithms are a class of statistical methods to sample from high-dimensional complex distributions (Andrieu and Thoms, 2008). The equilibrium state of MCMC, if the transition kernel warrants ergodicity, represents the target distribution.

In terms of the goodness-of-fit, the Watanabe-Akaike information criterion (WAIC) (Watanabe and Opper, 2010) is employed:

$$WAIC = -2\sum_{i=1}^{n}\log\left(E_{post}[p(y_i|\theta)]\right) + 2\sum_{i=1}^{n} Var_{post}(\log p(y_i|\theta)) \tag{29}$$

where the symbols E_{post} *and* Var_{post} denote mean and variances against the posterior distribution, respectively.

WAIC is stable because it has the desirable property of averaging over the posterior distribution rather than conditioning on a point estimate (Vehtari et al., 2017). A total of six commonly used joint distributions were selected in this research, and the expressions of specific functions are shown in Appendix 1 (Table A2).

3.3. Wildfire priority index

As described in the introduction, the direct application of the bivariate probability distribution for wildfire frequency analysis results in single mega-wildfire events and numerous wildfire activities being overlooked within normal burn areas. Accordingly, we used the weighted average method to obtain the probability of wildfire priority (WP) to balance the bivariate joint probability and univariate probability. The specific function is as follows:

$$WP = \alpha P_{XY}(X \leqslant x_i, Y \leqslant y_i) + \beta P_X(X \leqslant x_i) + \gamma P_Y(Y \leqslant y_i),\ \alpha + \beta + \gamma = 1 \tag{30}$$

where α, β, and γ are weighting coefficients. In Eq. (30), X represents log (LBA) and Y represents log(LFA). To ensure that there is enough weight in the joint extremes, this study sets α to 1/3. The values of α, β, and γ

will affect the assessed wildfire risk level. For example, a higher β value means that the burned area is considered to be more important in the wildfire bivariate characteristics. There, we use the line search (Nocedal and Wright, 1999) (step size is 0.01) to select the optimal β and γ. β is set to C*2/3, and γ is (1-C)*2/3. C is discrete from 0 to 1 in steps of 0.01. This study requires the wildfire priority index to perform better than bivariate joint probability in the case of super frequent wildfires and mega-wildfires. Therefore, the objective function (OF) is set to the sum of the proportion of the wildfire priority index that is better than the joint probability when the probability of log-burned-area is greater than 0.95 and when the probability of log-wildfire-activity is greater than 0.95. The specific objective function is as follows:

$$OF1 = \frac{numberof[P_{WP} - P_{XY}(X \leqslant x_i, Y \leqslant y_i)] > 0 \ when P_X(X \leqslant x_i) \geqslant 0.95}{numberof P_{F(x)}(x_i \geqslant X) \geqslant 0.95} \tag{31}$$

$$OF2 = \frac{numberof[P_{WP} - P_{XY}(X \leqslant x_i, Y \leqslant y_i)] > 0 \ when P_Y(Y \leqslant y_i) \geqslant 0.95}{numberof P_Y(Y \leqslant y_i) \geqslant 0.95} \tag{32}$$

$$OF = OF1 + OF2 \tag{33}$$

3.4. Representative sample selection

After calculating the probabilities of wildfire activity and burned area, as well as the wildfire priority index, we selected four representative sample points to further discuss the performance of our wildfire priority index in Results Section. Samples 1~3 represent wildfire types in wildfire extreme zone in Fig. 1. And sample 4 represents a general sample of wildifre. Sample 1, as a representative of super frequent wildfire, experienced 10 wildfire events within a month in February 2000. Sample 2 represents joint extreme wildfre, with frequent wildfire activity and a large burned area in April 1998. While for sample 3, it represents mega-wildfire. Sample 3 contains the largest mega-wildfire in California history from 1992 to 2018, namely, the Mendocino Complex Fire (Jia et al., 2020; Tentoglou et al., 2021). The total burned area due to the Mendocino Complex Fire reached almost 460 thousand acres, destroying over 280 businesses and homes (Yaloveha et al., 2019). Sample 4 from April 1995, as a general sample, came from non wildfire extreme zone.

3.5. Cluster analysis method

For the cluster analysis, all variables were normalized to prevent some variables with a wide range of changes from affecting the clustering results. The Mclust toolkit based on R was used for cluster analysis of the comprehensive dataset, which comprises three elements: (1) initialization via model-based hierarchical agglomerative clustering; (2) maximum likelihood estimation via the Expectation-Maximization (EM) algorithm (Bradley et al., 1998; Dempster et al., 1977); and (3) selection of the Bayesian model and the number of clusters using approximate Bayesian factors with the BIC approximation (Fraley and Raftery, 2002; Fraley et al., 2012; Scrucca et al., 2016). Unlike traditional clustering methods such as k-means clustering (MacQueen, 1967) and Ward's method (Ward Jr, 1963), the Mclust toolkit can address how many clusters there should be, which clustering method should be used, and how outliers should be handled. In particular, the Mclust toolkit entails the following four steps: It (1) determines the maximum number of clusters (M) and a set of mixture models to consider; (2) performs hierarchical agglomeration to approximately maximize the classification likelihood for each model and obtain the corresponding classifications for up to M; (3) applies the EM algorithm for each model and each number of clusters, starting with the classification from hierarchical agglomeration groups; and (4) computes the BIC approximation for the one-cluster case for each model and for the mixed model with the optimal parameters from EM for each cluster (Fraley and Raftery, 2002; Fraley et al., 2012; Scrucca et al., 2016). This study sets the maximum number of clusters (M) to 8, and 4 is selected as the optimal number of clusters in the final result. In addition, noise and outliers can be handled by iterative sampling, in which points of low probability are removed from the clusters and the clustering/removal process is repeated until all remaining observations have a relatively high density (Fraley and Raftery, 2002; Fraley et al., 2012; Scrucca et al., 2016).

3.6. Trend analysis method

The Mann-Kendall (MK) test, which was proposed by Mann (Mann, 1945) and modified by Kendall (Kendall, 1948), is widely used for analyzing the change trends in hydrometeorological time series (Liu et al., 2015; Yue and Wang, 2002). The advantage of the MK test is that the time series does not require any special form for the probability distribution function, which means it is less sensitive to potential interference from outliers in the data (Serrano et al., 1999). However, the test requires that the data be independent. Some hydrometeorological time series may usually display serial correlation, which will increase the probability that the MK test detects a significant trend, altering the estimated magnitude of the serial correlation (Yue and Wang, 2002). To efficiently eliminate the effect of the serial correlation on the MK trend test, Yue et al. proposed the trend-free prewhitening MK (TFPW-MK) test (Yue and Wang, 2002). Before the MK test, the time series are first detrended and prewhitened. The steps are listed in Appendix 1. And the trend can be classified according to the Z value (Table 1) (Wang et al., 2015).

4. Results

4.1. Performance capabilities of wildfire priority index

The optimal parameter C for the wildfire priority index is determined based on the selected univariate and bivariate joint probability distributions, as shown in Fig. 5. The value of the large parameter C means that more weight is given to the mega-wildfire. However, when the value of C exceeds 0.74, the objective function begins to decrease. In other words, the too-large parameter C will ignore most super frequent wildfires and further affect the ability of the wildfire priority index to assess wildfire risks. For details on the selection of functions for marginal distribution and joint distribution, please consult Appendix 2.

To compare the wildfire assessment ability of the optimal wildfire priority index in detail, Fig. 6 shows the difference between Joint, wildfire priority index-1 (Control group: α=1/3, β=1/3, and γ=1/3) and wildfire priority index-2 (Optimal group: α=1/3, β=74/150, and γ=26/150) in describing the wildfire risk through the probability and return

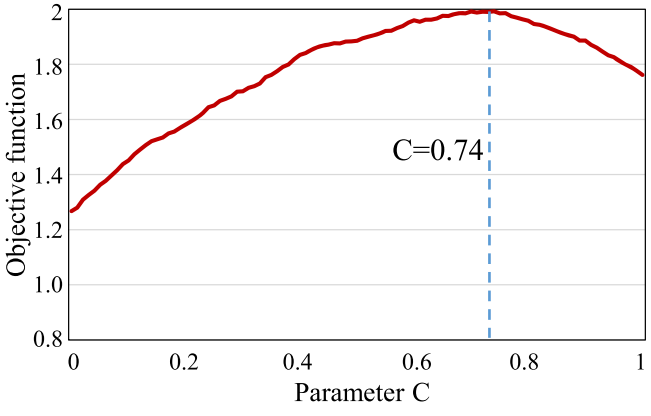

Fig. 5. Optimal curve of parameter C. When the parameter C = 0.74, the objective function has the optimal value.

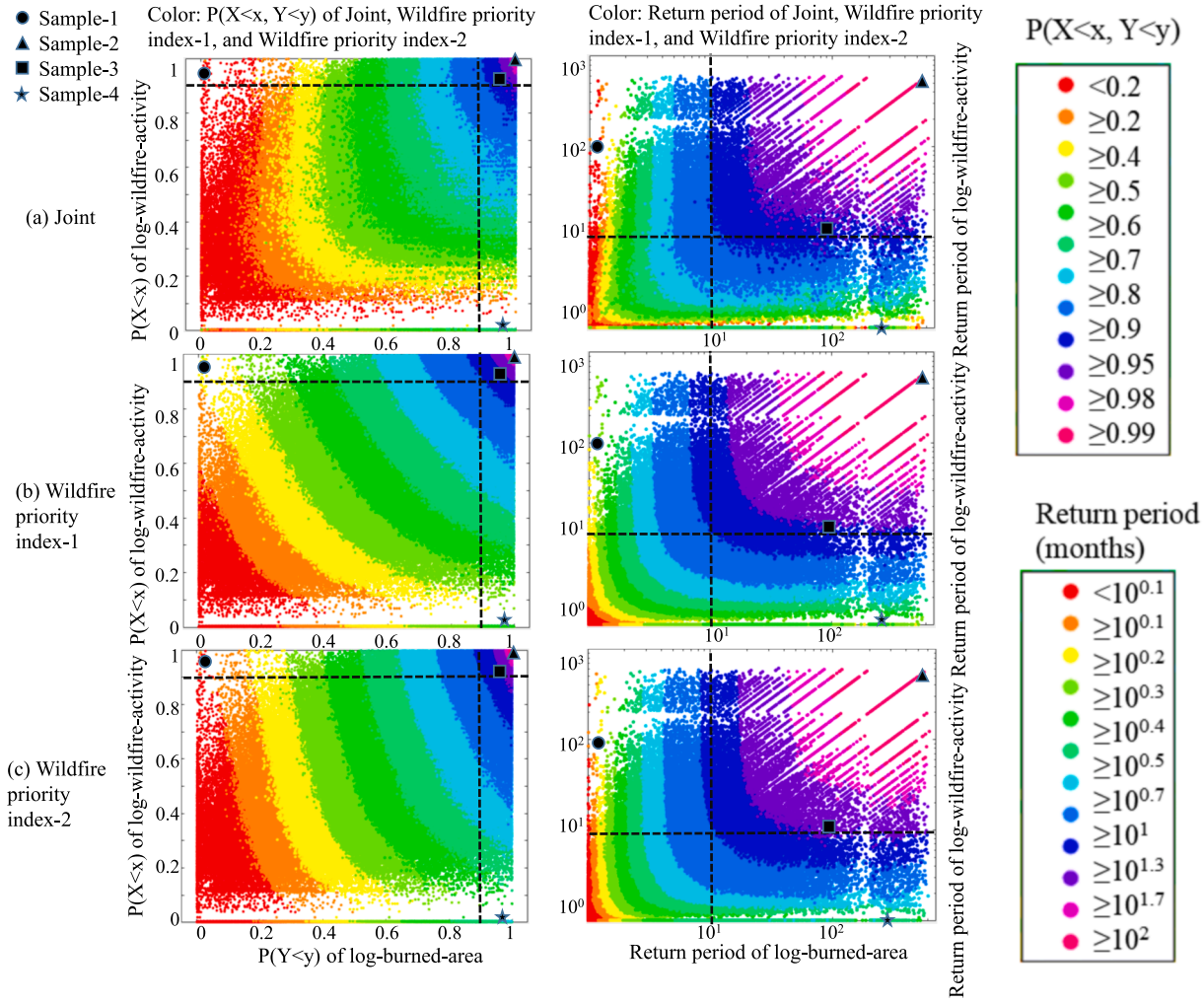

Fig. 6. Comparison of the probability and return period between Joint, wildfire priority index-1 and wildfire priority index-2. Wildfire priority index1 is the control group: α=1/3, β=1/3, and γ=1/3. Wildfire priority index-2 is the optimal group: α=1/3, β=74/150, and γ=26/150.

period. Additionally, this study selected four representative samples to evaluate the advantages and disadvantages of these three different methods. Fig. 6 demonstrates that the probability more sensitively measures the difference in extreme events (super frequent wildfires and mega-wildfires), while the return period is more sensitive to joint wildfire events. In other words, the probability can suitably represent the difference between Joint, wildfire priority index-1 and wildfire priority index-2 given the considered samples, while the return period is suitable for disaster risk trend analysis. Therefore, the P_{XY} of representative samples is listed in Table 2. Sample 1 represents super frequent wildfires resulting in a normal burned area. Ten wildfire events within a month in the grid of sample 1 in February 2000. The corresponding P_{XY} values of wildfire priority index-1 and wildfire priority index-2 are 39.47% and 24.16%, respectively. The wildfire priority index-1 indicates that the priority of super frequent wildfires is higher than that indicated by wildfire priority index-2, but both perform better than Joint. Given sample 2, which exhibits both a burned area and wildfire activity associated with a large return period value in April 1998, there is a minor difference in the performance of the return period between wildfire priority index-1 and wildfire priority index-2, reaching more than 99% of P_{XY}. The advantage of focusing on mega-wildfires is more significant in wildfire priority index-2 when considering sample 3. The probability of sample 3 (mega-wildfire) considering Joint and wildfire priority index-1 is still lower than 50%, indicating that these two methods are insufficient in the assessment of mega-wildfires. In contrast, the probability of wildfire priority index-2 is 65.49%, which is significantly higher than that of Joint and wildfire priority index-1. Sample 4 attained a P_{XY} value of 98.86% for the burned area and a P_{XY} value of 90.00% for the wildfire activity. The burned area of sample 4 (came from non wildfire extreme zone) in April 1995 reached 34 thousand acres, which was the second-largest fire in the history of this sample. The performance of wildfire priority index-2 is also better than that of wildfire priority index-1, reaching a probability of 94.03%. Overall, both the wildfire priority index-1 and wildfire priority index-2 perform better than Joint in assessing wildfire conditions. In particular, the

Table 2
P_{XY} of the four representative samples. The locations of the four sample points are shown in Figure 3(b).

	P of log-burned-area	P of log-wildfire-activity	P of Joint	P of wildfire priority index-1	P of wildfire priority index-2	Date
Sample 1	2.14%	97.86%	18.42%	39.47%	24.16%	02/2000
Sample 2	98.93%	99.64%	98.78%	99.12%	99.00%	04/1998
Sample 3	99.50%	0.50%	48.95%	49.65%	65.49%	07/2018
Sample 4	98.86%	90.00%	88.97%	92.61%	94.03%	04/1995

advantage of wildfire priority index-2 is that mega-wildfires are assigned a higher priority.

4.2. Performance capabilities with different probabilities

In order to effectively evaluate the relationship between hydrometeorology and wildfire behavior, it is imperative to first establish a classification system for the five identified wildfire types. This paper selected marginal probabilities and joint probabilities combined with marginal probabilities as control groups to compare the differences in assessing the hydrometeorology-wildfire relationship under different probability calculation methods. Regarding the control groups, the threshold probabilities were primarily influenced by the extent of the burned area, which was a critical factor in both WT1 and WT2. Due to the limited research on wildfire based on probability frameworks, we referred to the probability threshold of 0.99 for defining extreme high-temperature events and extreme rainfall events when selecting the probability threshold for extreme fire events (Myhre et al., 2019; Thackeray et al., 2022). In addition, as WT1 is defined as a type of wildfire with a large burned area but minimal wildfire activity, the probability of wildfire activity for WT1 was set to less than 0.3. The reason for not choosing a threshold of 0.2 or 0.1 here was that there were no WT1 fires in the entire study area. As the wildfire activity increases, WT1 gradually transitions to WT2. For WT2, wildfire activity near the 0.5 probability was selected, i.e., fire activity probabilities between 0.45 and 0.55. The same approach was used for WT4 and WT5. WT3 indicates that both the burned area and wildfire activity reached extremes, so the probability threshold for both was 0.99. For the experimental group, the univariate probabilities were selected according to the same principles as the control group. For the joint probability, WT3 indicated the extreme condition and thus had a joint probability threshold of 0.99. WT1, WT2, and WT3 have the same threshold of burned area, and their probability threshold for wildfire activity represent near the minimum value, near the median value, and near the maximum value, respectively. The same is true for the threshold of burned area for WT5, WT4, and WT3. For the experimental group, the threshold range was adjusted several times for WT1, WT2, WT4, and WT5, and the three experimental groups achieved the most similarity to the control group when the final probability thresholds were within the range in Table 3.

Based on the probability threshold in Table 3, Fig. 7 shows the comparison results for the experimental and control groups, with different colors indicating the median probability of weather values. For specific measurements of performance, in fact, we have used the average absolute value of difference (AAD) under different types of wildfires. For example, for WT1, the probability of each meteorological variable joint in the experimental group is subtracted from the probability of each meteorological variable joining the experimental group, and then calculate the average absolute value of the difference. WP2 was most similar to the control group, especially in WT1 and WT2, where the burned area was the dominant element. WP2 performed significantly better than WP1 and the joint, especially when measuring the relationship between the hydrometeorological variables and WT1, which was also consistent with the findings in Result 4.1. For WT3, there was no significant difference between the three experimental groups. Additionally, WP1 and WP2 also outperformed the joint for WT4. In conclusion, by comparing the probabilities calculated under the different methods, WP2 was found to outperform the other two methods. Therefore, WP2 was used to classify the wildfire types in all subsequent analyses.

Table 3
Probability thresholds for wildfire classification. X and Y correspond to log(LBA) and log(LFA).

Types	Control Group	Experimental Group		
		Joint (direct application of joint probability)	WP1 (wildfire priority index-1)	WP2 (wildfire priority index-1)
WT1 (mega-wildfire)	$P_X>0.99$ $P_Y<0.30$	$P_X>0.99$ $0.7<P_{Joint\ or\ WP1\ or\ WP2}<0.8$		
WT2 (joint wildfire-1)	$P_X>0.99$ $0.45<P_Y<0.55$	$P_X>0.99$ $0.8< P_{Joint\ or\ WP1\ or\ WP2}<0.9$		
WT3 (joint extremes)	$P_X>0.99$ $P_Y>0.99$	$P_{Joint\ or\ WP1\ or\ WP2}>0.99$		
WT4 (joint wildfire-2)	$P_Y>0.99$ $0.45<P_X<0.55$	$P_Y>0.99$ $0.8< P_{Joint\ or\ WP1\ or\ WP2}<0.9$		
WT5 (super frequent wildfires)	$P_Y>0.99$ $P_X<0.30$	$P_Y>0.99$ $0.7< P_{Joint\ or\ WP1\ or\ WP2}<0.8$		

4.3. Overall wildfire conditions in the United States

Based on the classification method of WP2, the seasonal distribution of the five wildfire types is shown in Fig. 8 and Fig. 9. WT1 and WT5 showed significant seasonality. WT1 was mainly concentrated in summer (39.1% of the total), while WT5 corresponded to spring (35.7% of the total). For WT2 and WT4, the wildfire was dominant in autumn, accounting for 33.9% and 30.0% respectively. However, for WT3, it has a high proportion in spring and summer, with 32.3% and 32.5% respectively. In fact, in the United States, especially in the eastern United States, there is much wildfire activity (especially human-caused wildfires) in the spring (Balch et al., 2017; Nagy et al., 2018). On the other hand, of the 43 notable mega-wildfires in the United States (Buckland, 2019), 33 wildfires occurred in the summer, and July accounted for 42.2% of the summer mega-wildfires.

To further understand the hydrometeorology-wildfire relationship in the United States, the probabilities of the hydrometeorological variables under different wildfire types are tabulated in Fig. 10. A higher probability indicated drier (less precipitation and lower SPEI, PDSI, or SSM values), hotter weather, and stronger wind speeds. For WT1, known as mega-wildfire, dry soil and lack of precipitation (SMM and PRE) were two of the main causes of severe wildfires, which were also favorable conditions for fuel accumulation. There are no particularly high meteorological element probability values (greater than 0.7) in WT2. However, this does not suggest that there is no relationship among hydrometeorological variables between WT2 but rather that wildfires are often subject to a combination of meteorological elements in locations that are dominated by large burned areas. For the other three wildfire types, three significant high-probability variables could be identified, specifically WT3 dominated by SPEI, PRE, and TEM; WT4 dominated by SSM, SPEI, and PRE; and WT5 dominated by SSM, PRE, and TEM. Compared to a regular wet and rainy spring, a warm and dry spring dominated by a high probability of SSM, PRE, and TEM created natural conditions for frequent wildfire activity, i.e., WT5. There are two possible reasons for the differences in the performance of SSM, PDSI, and SPEI for WT4 and WT5. One reason is that the differences in the performance of different drought indices are mainly due to their different calculation processes and represented physical processes. SSM, as a soil drought index, can affect the moisture content of dead fuel. PDSI and SPEI are both representatives of meteorological drought indices. Another reason is that WT4 and WT5 are both types of wildfires dominated by wildfire activity. The occurrence of wildfires is more susceptible to the influence of fuel. And SMM not only affects the fuel moisture content but also affect the accumulation of fuel, so SSM performs better on WT4 and WT5 than PDSI and SPEI.

4.4. Hydrometeorology-wildfire relationship in different ecoregions

The hydrometeorological conditions and vegetation characteristics

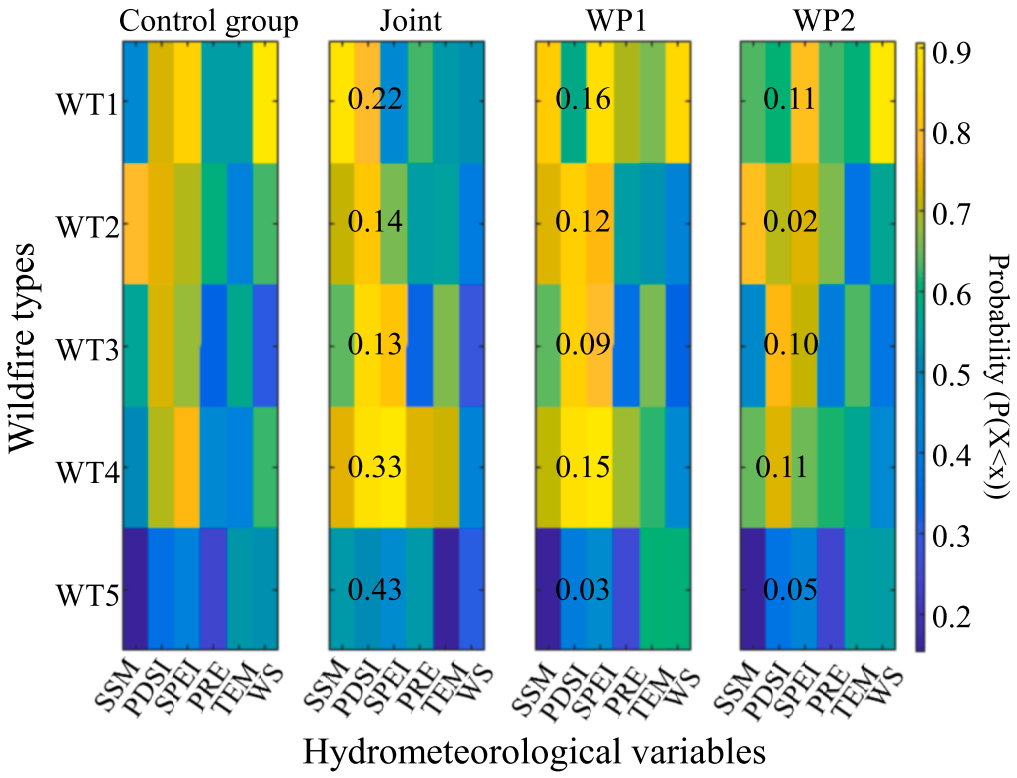

Fig. 7. Comparison of the performance of the Joint, WP1, and WP2 methods in assessing the impact of weather elements using the wildfire bivariate statistical characteristics framework. The numbers in the graph represent the average absolute difference between the probability of hydrometeorological variables in the experimental group and the probability of meteorological elements in the control group.

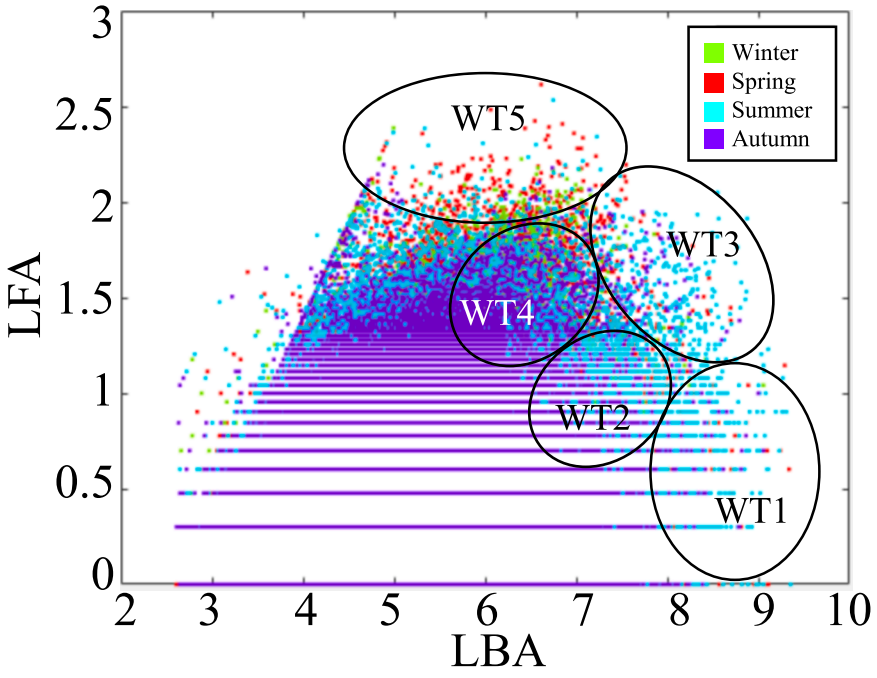

Fig. 8. Seasonal distribution of wildfires in the U.S. LBA: log-burned area, LFA: log-wildfire activity.

exhibit significant variability across the diverse ecoregions of the United States. To elucidate the intricate interplay between these factors, Figs. 11-13 provide a detailed representation of the relationships between hydrometeorological variables and wildfire within each ecoregion (The enlarged versions of Figs. 11-13 can be seen in Appendix 1). These analyses are further stratified by season and temporal variations. The seventeen ecoregions under study can be categorized into three distinct groups, based on the diversity of wildfire types they

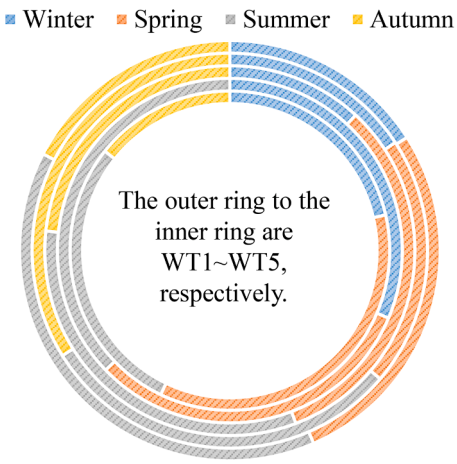

Wildfire type \ Season	Winter	Spring	Summer	Autumn
WT1	15.9%	27.5%	39.1%	17.4%
WT2	15.8%	20.5%	29.8%	33.9%
WT3	11.9%	32.3%	32.5%	23.3%
WT4	19.3%	25.3%	25.3%	30.0%
WT5	21.4%	35.7%	28.6%	14.3%

Fig. 9. The proportion of different types of wildfires in four seasons. The circular diagram on the left represents WT1~WT5 from the outer ring to the inner ring, respectively.

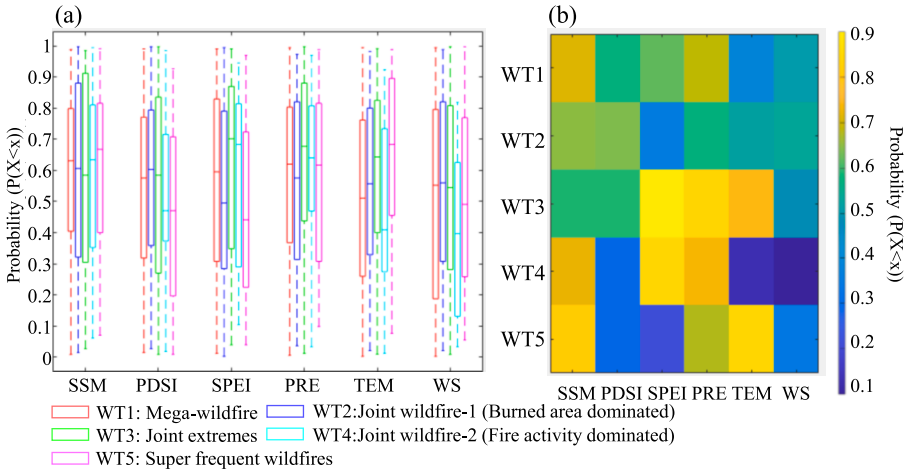

Fig. 10. Average probability (P($X < x$)) of meteorological values under the five fire types in the U.S.: (a) Overall conditions; and (b) Median value.

encompass: (1) ecoregions that exhibit all five identified wildfire types, (2) ecoregions where four wildfire types are present, lacking super frequent wildfires (WT5), and (3) ecoregions that are characterized by the presence of three or fewer wildfire types.

Across six ecoregions, all wildfire types were observed (the Western Sierra Madre Piedmont and Warm Deserts, Western Cordillera, Southeastern Plains, Ozark Ouachita-Appalachian Forests, Mississippi Alluvial and Southeastern Coastal Plains, and West-Central Semi-Arid Prairies). Notably, in the Western Sierra Madre Piedmont and Warm Deserts, WT5 predominantly occurred during the summer of 1992–1999, largely driven by high temperatures. This ecoregion experienced a decline in extreme wildfires, with no WT1 or WT5 recorded from 2010 to 2018. In both the Ozark Ouachita-Appalachian Forests and West-Central Semi-Arid Prairies, strong winds facilitated the spread of WT5 (mega-wildfires). However, the dominant factors of WT3 differed between these ecoregions: PDSI in the Ozark Ouachita-Appalachian Forests and both PRE and WS in the West-Central Semi-Arid Prairies. The WT2 in the Southeastern Plains was marked by high-probability hydrometeorological variables, with low precipitation and drought (particularly SPEI) favoring WT2 conditions. The Mississippi Alluvial and Southeastern Coastal Plains saw a notable PRE-WT1 correlation. In the Western Cordillera, extreme temperatures predominated for WT4 and WT5, with a significant uptick in extreme wildfire events from 2010 to 2018, and WT2 and WT4 occurring in all seasons.

Seven ecoregions, specifically Cold Deserts, Mediterranean California, Mixed Wood Shield, Marine West Coast Forest, Mixed Wood Plains, Temperate Prairies, and South-Central Semi-Arid Prairies, were identified as lacking super frequent wildfires (WT5). In these regions, certain ecoregions exhibited a high probability of specific hydrometeorological variables influencing WT1 wildfires. These include PDSI-SSM-WT1 in Cold Deserts, PRE-WT1 in Mixed Wood Shield, PDSI-SPEI-WT1 in Temperate Prairies, and PRE-WS-WT1 in South-Central Semi-Arid Prairies. In the remaining three ecoregions, dominant hydrometeorological variables were linked to WT2, with TEM-WT2 in Mediterranean California, SSM-SPEI-WT2 in Marine West Coast Forest, and TEM-WT2 again in Mixed Wood Plains. Furthermore, the occurrence of WT1, WT2, WT3, and WT4 in Mixed Wood Shield, Marine West Coast Forest, and Mixed Wood Plains was confined to the period from 2010 to 2018.

Among the four other ecoregions, the Upper Gila Mountains, Atlantic Highlands, Central Plains, and Texas-Louisiana Coastal Plain and Tamaulipas-Texas Semiarid Plain, joint extremes existed only in the Central Plains. The vegetation cover of the Central Plains is mainly grassland, and wildfire activity and burned area have a strong correlation, with a high probability of wildfire activity and burned area often occurring simultaneously. The dominant combinations of hydrometeorological-wildfire relationships in the other three ecoregions were WT1 with PDSI in the Upper Gila Mountains, WT1 with WS in the Atlantic Highlands, and WT2 with TEM in the Texas-Louisiana Coastal Plain and Tamaulipas-Texas Semiarid Plain.

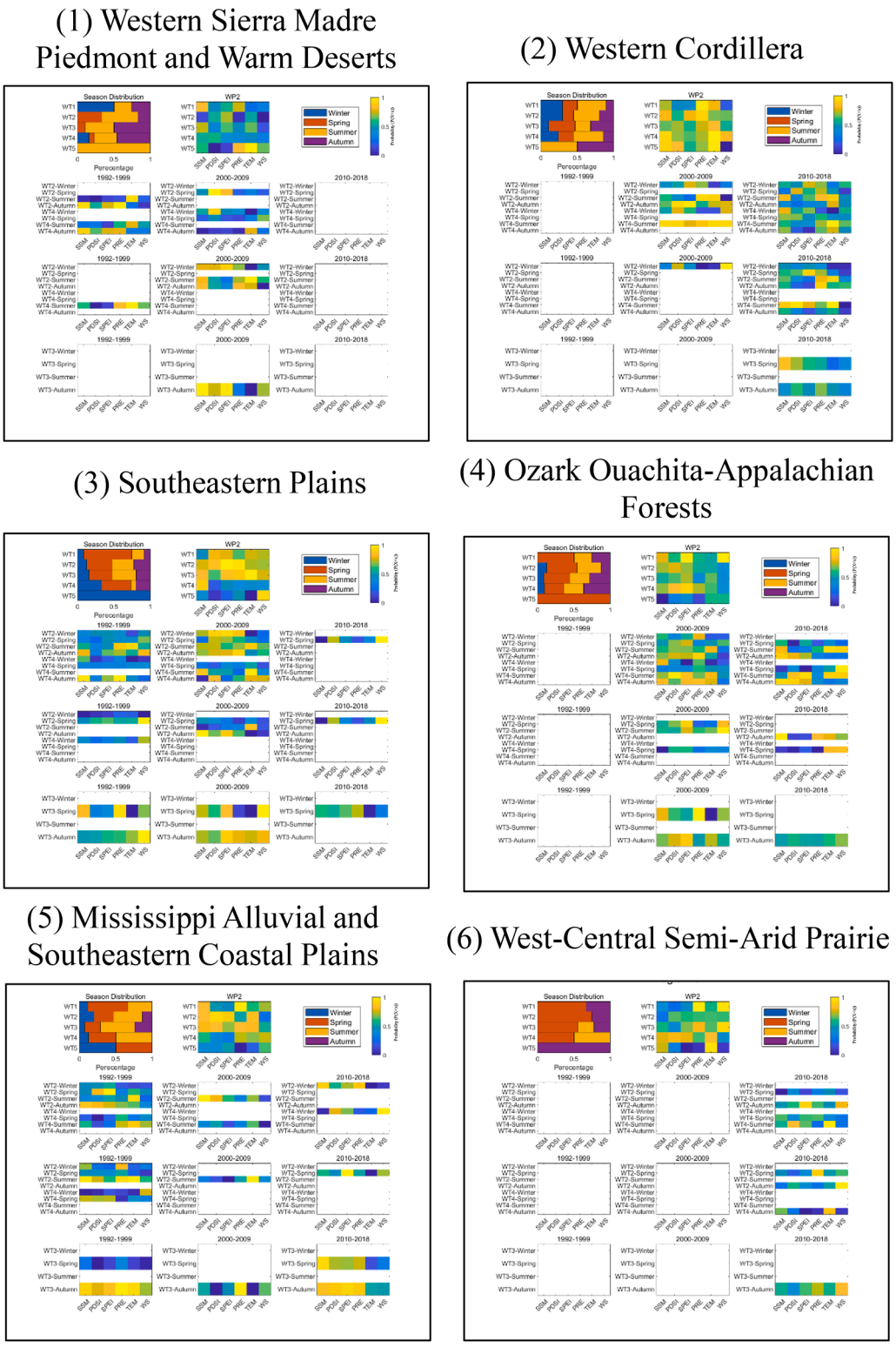

Fig. 11. Median probability ($P(X < x)$) of meteorological factors in ecological regions 1–6 in different seasons and years.

In addition, we focused on the seasonal variation in wildfires, for example, in Mediterranean California and the Ozark Ouachita-Appalachian Forests the season of occurrence of oversized fires shifted from spring and summer to autumn and low soil moisture content was dominant in autumn. In other words, the impact of extreme autumn drought on mega-fires increased. Both WT2 and WT4 in Mediterranean California had the same second dominant factor, i.e., wind, but WT4 could change to WT2 when the first dominant factor changed from PRE to TEM. A similar situation was found in the Ozark Ouachita-Appalachian Forests, where WT2 could also change to WT4 when the dominant factor changed from PDSI combined with SPEI to PDSI combined with SSM. This revealed that joint wildfires are influenced by similar factors and that changes in meteorological elements at different times can cause joint wildfires to transition between WT2 and WT4.

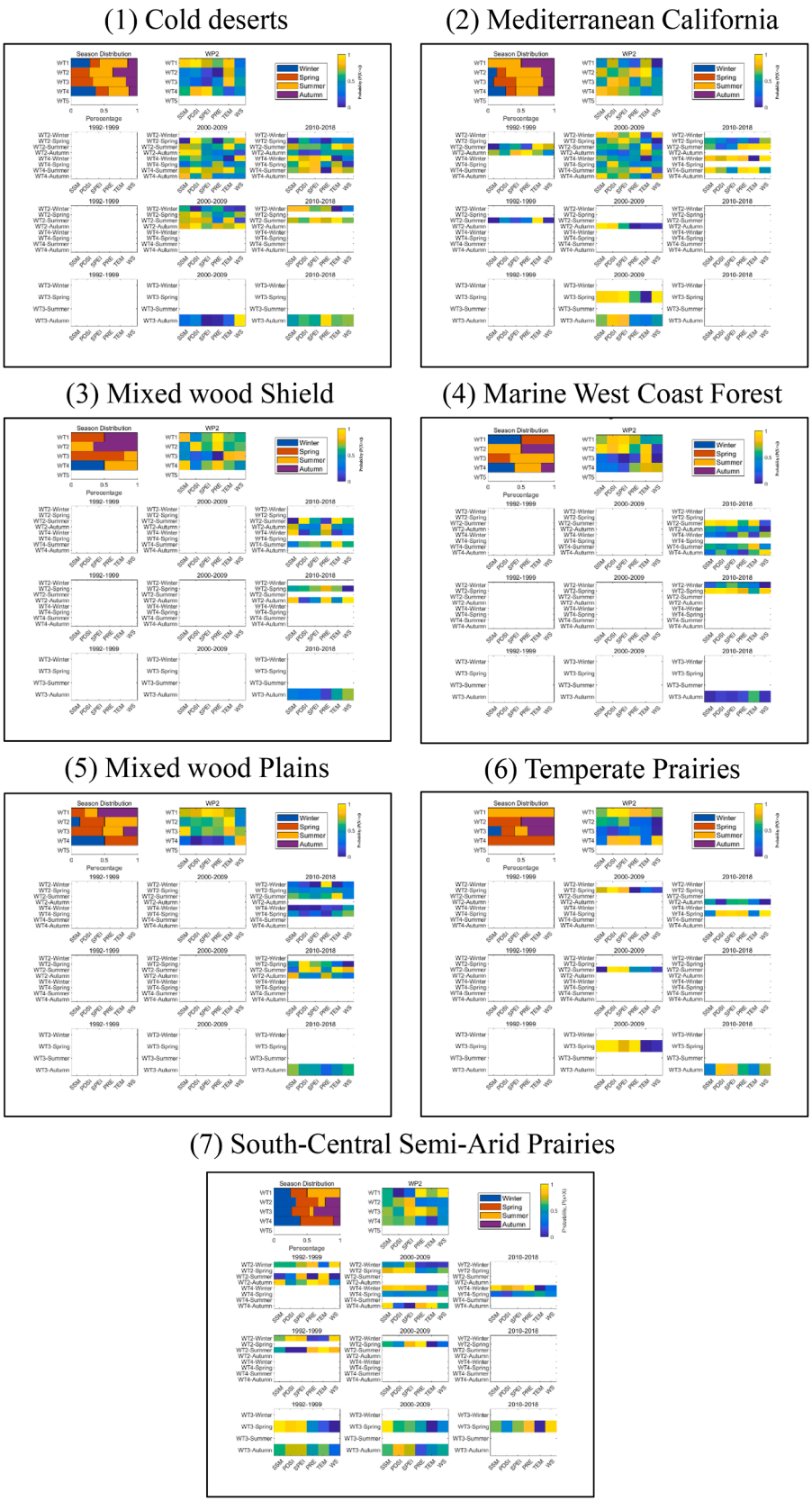

Fig. 12. Median probability (P($X < x$)) of meteorological factors in ecological regions 7–13 in different seasons and years.

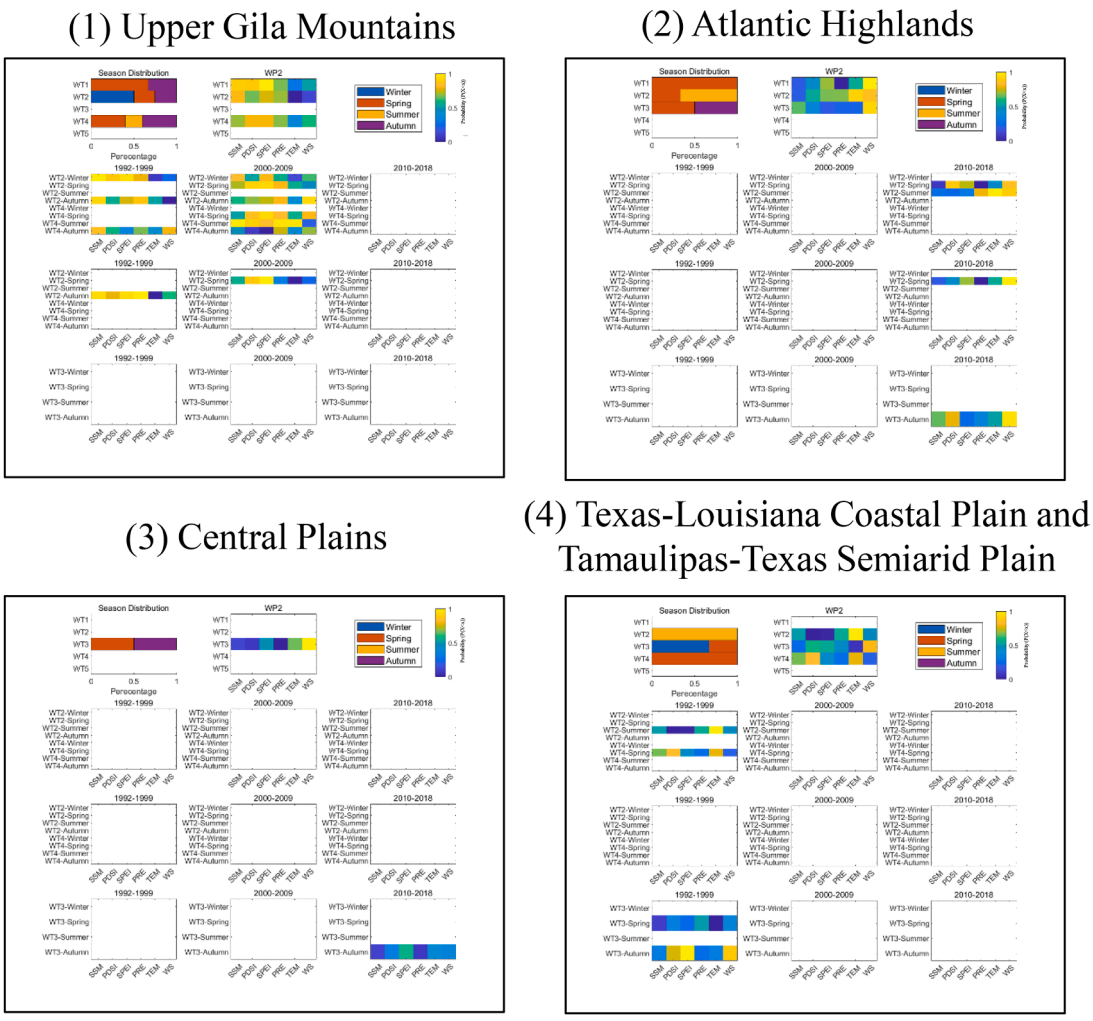

Fig. 13. Median probability (P($X < x$)) of meteorological factors in ecological regions 14–17 in different seasons and years.

4.5. Spatiotemporal characteristics of wildfire statistics

The hydrometeorology-wildfire relationships within the 17 ecoregions presented too much information. To further extract valid information and thus provide guidance for wildfire prevention, the median of the distribution for hydrometeorological values under each wildfire type were used as input (missing fire types were input as 0) to obtain four new clusters, as shown in Fig. 14. Specifically, cluster 1 contained Mediterranean California, Cold deserts, South-Central Semi-Arid Prairies, Mixed wood Shield, Atlantic Highlands, Mixed wood Plains, with multiple

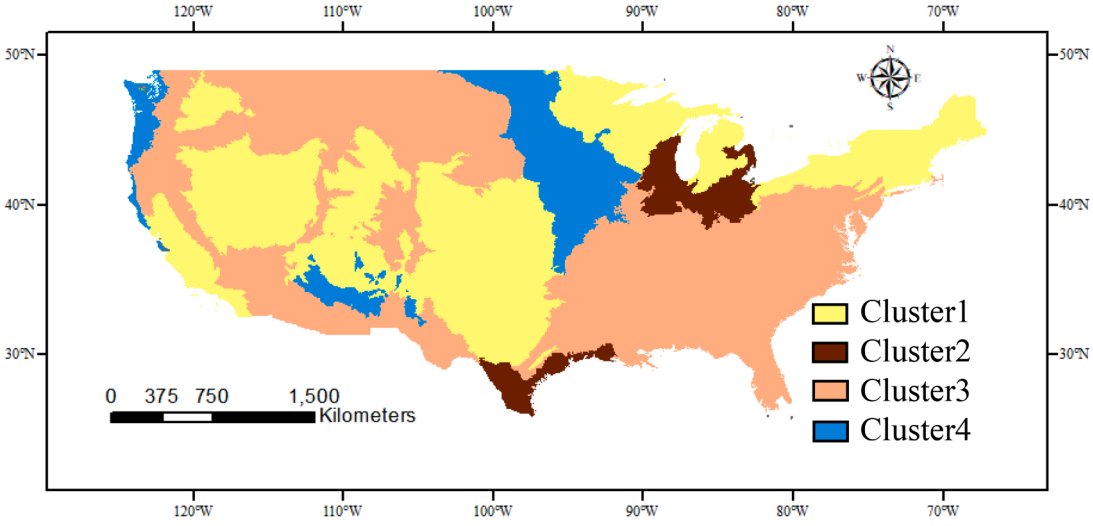

Fig. 14. Clustering zones of ecoregions based on the probability of meteorological factors.

vegetation types. Cluster 2 contained two ecoregions, the Central Plains and the Texas-Louisiana Coastal Plain and Tamaulipas-Texas Semiarid Plain, where the vegetation cover is mainly cultivated crops and hay. Cluster 3 includes 7 ecological zones, such as Upper Gila Mountains, Western C'ordillera, etc. There are also many types of vegetation in Cluster 3, mainly including evergreen forests and deciducous forests. Marine West Coast Forest and Temperate Prairies form the cluster 4 where the vegetation cover is mainly cultivated crops and evergreen forests. This cluster partitioning divided the original classification of ecoregions that considered only vegetation and climatic characteristics. Considering the relationship between hydrometeorology and wildfire through classification is more instructive for wildfire research. For example, unlike other plain types, the wildfire activity and burned area within cluster 2 had a strong correlation, and WT1 and WT5 were completely absent from these two ecoregions.

From Fig. 15 (The enlarged versions of Fig. 15 can be seen in Appendix 1), among the four clusters, only cluster 3 had all wildfire types, and cluster 2 had only three types of wildfires: WT2, WT3, and WT4. The most significant combination of all the combinations of wildfire type and hydrometeorological variables in both cluster 1 and cluster 2 was WT2-TEM. In cluster 3, the dominant roles of the SPEI and PDSI for WT2 prevailed. The dominant role of the SPEI and PDS in cluster 4 was reflected in WT1.

Additionally, by analyzing the trend of the hydrometeorological variables in all the clusters and extracting the top two variables with the highest probability (as shown in Fig. 16), it could be seen that drought showed an intensifying trend among the hydrometeorological variables in cluster 1. Cluster 4 was similar to cluster 1 and also has increased drought concerns. The hydrometeorological variables in cluster 2 showed no significant change trend. Multiple extreme hydrometeorological variables (stronger winds, drier weather, higher temperatures) intensified simultaneously in cluster 3.

5. Discussions

This paper mainly focuses on the bivariate characterization of wildfire that considers both burned area and wildfire activity, rather than the univariate wildfire cause analysis that most scholars have paid attention to in the past. Although there are many studies on wildfire in the continental United States, the analysis framework based on the bivariate characteristics of wildfires proposed in this paper for the first time can reduce two-dimensional variables to one-dimensional comprehensive consideration (Abatzoglou and Kolden, 2013; Margolis and Swetnam, 2013; Riley et al., 2013). In particular, the wildfire priority index (especially the wildfire priority index-2) provided in this study can offer a new way to identify high wildfire-risk regions. On the one hand, since the wildfire priority index is based on the probability of each grid cell, the index value can be compared between different grid cells. Even with the same burned area or wildfire activity, Evergreen Forests in California and Herbaceous in the plains of the western continental United States can have varying degrees of wildfire risk. However, the corresponding probability values for the two regions will be different and thus can be compared. On the other hand, the wildfire priority index provides global characteristics of wildfire conditions. For example, within the same grid cell, the burned area and wildfire activity characteristics vary greatly between different months. In the sample-2

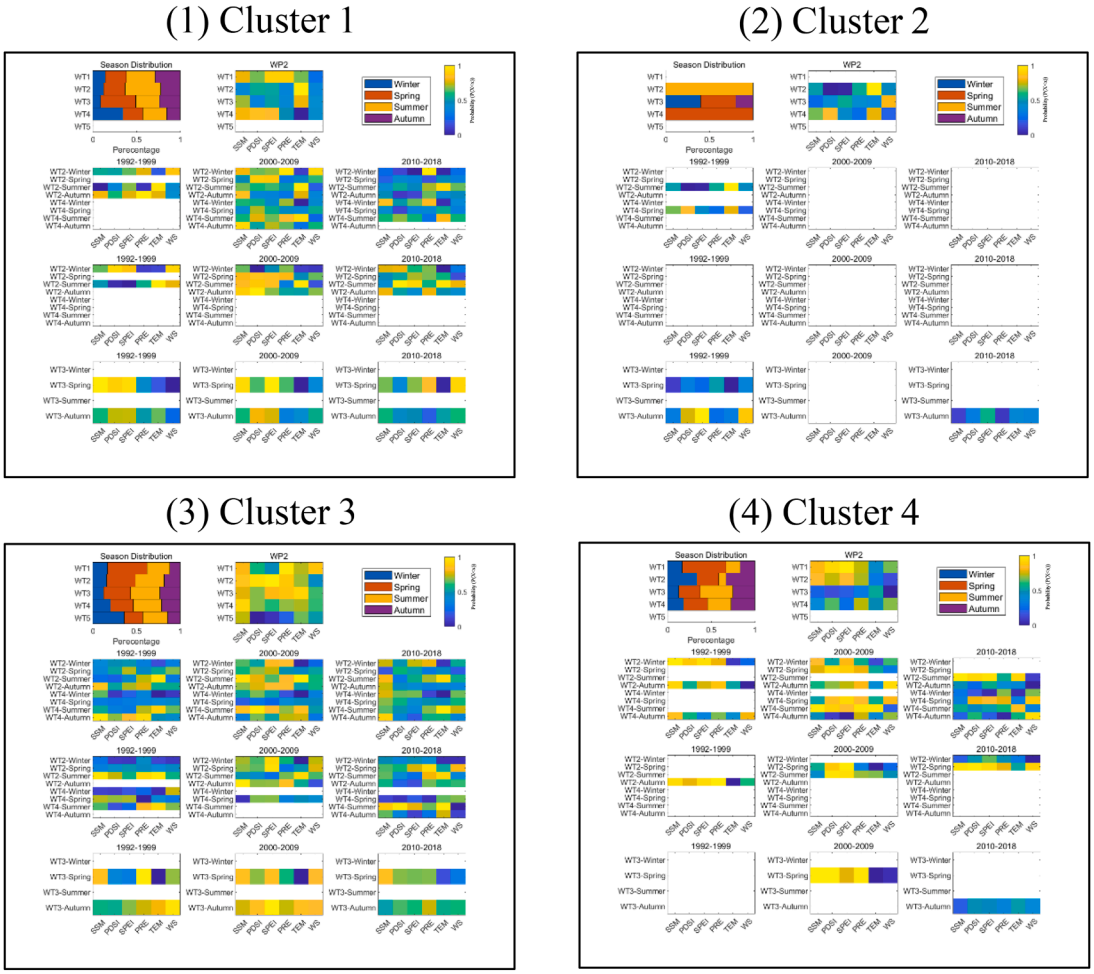

Fig. 15. Probability of meteorological factors in the clustering zones.

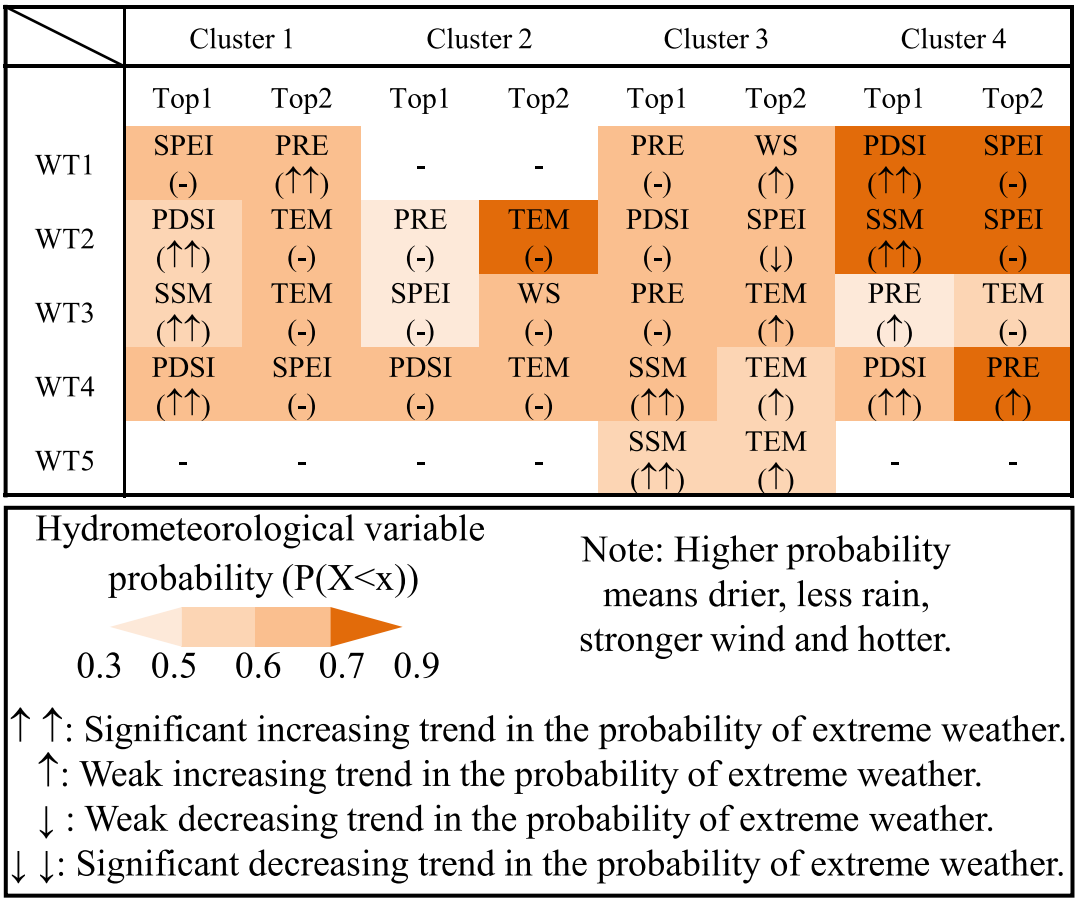

Fig. 16. The top two dominant meteorological factors in the clustering zones.

grid cell, there were 19 wildfire events in September 1992 with the burned area of 2.5 ha, while in September 2003 there were 5 wildfire events with the burned area of 14.4 ha. In this case, using only the burned area or the wildfire activity may result in the opposite degree of risk for wildfires, while the wildfire priority index can take into account wildfire bivariate characteristics to assess wildfire risk more comprehensively. In addition, through the trend analysis of the return period calculated by the wildfire priority index, the regions that need to be focused on in the future can be obtained. Compared with the wildfire events that have occurred, the changing trend of future wildfire risks will be more instructive for fire management.

Furthermore, based on the identification of different types of wildfires, more targeted wildfire prevention and control measures can be taken. For example, for mega-wildfire (WT1), fuel treatments and human-controlled open burning as a process to increase resistance to high-severity wildfires could provide a viable option for slowing vegetation change and the associated impacts on carbon cycling and biodiversity over larger areas (Hurteau et al., 2014). On the other hand, for super frequent wildfires (WT5), broad-scale reduction of human-caused ignitions and the redistribution of fire-dependent forest types away from human ignition sources (Sturtevant et al., 2009). In addition, based on the possible changes in wildfire types discovered in this study, it becomes even more important to flexibly adjust wildfire prevention strategies instead of adopting an unchanging strategy according to the changes in dominant wildfire types in the wildfire regime.

6. Conclusions

Unlike previous studies that considered burned area and wildfire activity separately in their wildfire regime classifications (Brewer et al., 2005; Malamud et al., 2005; Trucchia et al., 2022), we present the first wildfire type classification based on the wildfire bivariate statistical characteristics in this paper. On this basis, the influence of hydrometeorological variables on different wildfire types was examined in the United States during 1992~2018. From the results, the major conclusions and limitations were as follows:

(1) In this paper, wildfires were classified into five types using the bivariate statistical characteristics of wildfire: WT1 (mega-wildfire), WT2 (joint wildfire-1 (burned area dominated)), WT3 (joint extremes), WT4 (joint wildfire-2 (fire activity dominated)), and WT5 (super frequent wildfires). In the United States as a whole, WT1 and WT2 were affected by multiple weather elements and their causes were more complicated, while WT5 was mainly affected by soil moisture, precipitation, and temperature.

(2) The influence of hydrometeorological variables on different wildfire types was discussed in 17 ecoregions. The most dominant combinations of hydrometeorological variables and wildfire types in the 17 ecoregions were PDSI-WT1 in the Cold deserts, TEM-WT2 in Mediterranean California, TEM-WT5 in the Western Sierra Madre Piedmont and Warm Deserts, SPEI-WT1 in the Upper Gila Mountains, PRE-WT1 in the Mixed wood Shield, WS-WT1 in the Atlantic Highlands, PRE-WT1 in the Western Cordillera, SPEI-WT2 in the Marine West Coast Forest, TEM-WT2 in the Mixed wood Plains, WS-WT3 in the Central Plains, SPEI-WT2 in the Southeastern Plains, WS-WT1 in the Ozark Ouachita-Appalachian Forests, PRE-WT1 in the Mississippi Alluvial and Southeastern Coastal Plains, PDSI-WT1 in the Temperate Prairies, TEM-WT5 in the West-Central Semi-Arid Prairies, SPEI-WT2 in the South-Central Semi-Arid Prairies, and TEM-WT2 in the Texas-

Louisiana Coastal Plain and Tamaulipas-Texas Semiarid Plain. Additionally, changes in hydrometeorological variables in different periods could lead to mutual conversion between WT2 and WT4.

(3) In the four new clusters, intensifying droughts are a concern in clusters 1 and 4, while there are multiple concerns in cluster 3, namely, stronger winds, higher temperatures, and more drought.

(4) There remain a few limitations in describing the bivariate characteristics of wildfire. Wildfire statistics do not yield long-term continuous time series similar to other traditional hydrometeorological data. It is also common that no wildfire occurs for several months in a high-rainfall year. Even though grid cells with fewer than 100 valid data points were removed in this study, the data length remains an unavoidable source of uncertainty in frequency analysis. The generation of longer data series or reconstruction of wildfire events through paleoclimate research can provide more reliable data for wildfire frequency analysis.

(5) An additional limitation of the wildfire classification analysis presented in this article is the omission of human influences in its consideration, such as wildfire management, wildfire suppression, wildfire prevention, and fuel treatments. Considering human influences on wildfire will be critical in future research. In wildfire forecasting, atmospheric-oceanic indices and hydrometeorological elements and indicators such as GDP and population density need to be considered as predictor variables.

Overall, even though our study focused only on bivariate statistical characteristics of wildfire, it also provided a new way of thinking about other compound hazards in the face of climate change. Research on compound hazards such as compound droughts and hot extremes (Hao et al., 2018) and compound wildfires and COVID-19 (Navarro et al., 2021) has surfaced in recent years. By applying the analytical framework of compound hazards in this paper, the understanding of other types of compound hazards can also be improved.

CRediT authorship contribution statement

Ke Shi: Writing – review & editing, Writing – original draft, Methodology, Formal analysis. **Yoshiya Touge:** Writing – review & editing, Supervision, Resources, Funding acquisition. **So Kazama:** Writing – review & editing, Supervision, Resources.

Declaration of competing interest

The authors declare that they have no known competing financial interests or personal relationships that could have appeared to influence the work reported in this paper.

Data availability

All data used in this study are freely available online. The wildfire data is publicly available at https://www.fs.usda.gov/rds/archive/Catalog/RDS-2013-0009.5. The hydrometeorological data can be obtained from https://cds.climate.copernicus.eu/cdsapp#!/dataset/reanalysis-era5-single-levels?tab=overview.

Acknowledgments

This work was conducted by Theme 4 of the Advanced Studies of Climate Change Projection (SENTAN Program) Grant Number JPMXD0722678534, Grant-in-Aid for Scientific Research (A), 2024–2027 (24H00336; Yoshiya Touge), Grant-in-Aid for Scientific Research (B), 2020–2023 (20H02248; Yoshiya Touge), and Grant-in-Aid for Scientific Research (A), 2020–2023 (20H00256, So Kazama) supported by the Ministry of Education, Culture, Sports, Science and Technology (MEXT), Japan.

Supplementary materials

Supplementary material associated with this article can be found, in the online version, at doi:10.1016/j.agrformet.2024.110215.

References

Abatzoglou, J.T., Kolden, C.A., 2013. Relationships between climate and macroscale area burned in the western United States. Int. J. Wildland. Fire 22 (7), 1003–1020.
Abramowitz, M. and Stegun, I.A., 1964. Handbook of mathematical functions with formulas, graphs, and mathematical tables, 55. US Government printing office.
Aldersley, A., Murray, S.J., Cornell, S.E., 2011. Global and regional analysis of climate and human drivers of wildfire. Sci. Total Environ. 409 (18), 3472–3481.
Allen, R.G., Pereira, L.S., Raes, D., Smith, M., 1998. Crop evapotranspiration-Guidelines for computing crop water requirements-FAO Irrigation and drainage paper 56. Fao, Rome 300 (9), D05109.
Andela, N., et al., 2017. A human-driven decline in global burned area. Science 356 (6345), 1356–1362.
Andrews, P.L., Cruz, M.G., Rothermel, R.C., 2013. Examination of the wind speed limit function in the Rothermel surface fire spread model. Int. J. Wildland. Fire 22 (7), 959–969.
Andrieu, C., Thoms, J., 2008. A tutorial on adaptive MCMC. Stat. Comput. 18 (4), 343–373.
Balch, J.K., et al., 2017. Human-started wildfires expand the fire niche across the United States. Proc. Natl. Acad. Sci. 114 (11), 2946–2951.
Bartsch, A., Balzter, H., George, C., 2009. The influence of regional surface soil moisture anomalies on forest fires in Siberia observed from satellites. Environ. Res. Lett. 4 (4), 045021.
Beguería, S., Vicente-Serrano, S.M., Reig, F., Latorre, B., 2014. Standardized precipitation evapotranspiration index (SPEI) revisited: parameter fitting, evapotranspiration models, tools, datasets and drought monitoring. Int. J. Climatol. 34 (10), 3001–3023.
Bhatti, S.J., Kroll, C.N., Vogel, R.M., 2019. Revisiting the probability distribution of low streamflow series in the United States. J. Hydrol. Eng. 24 (10), 04019043.
Bowman, D.M., et al., 2009. Fire in the Earth system. Science 324 (5926), 481–484.
Bradley, P.S., Fayyad, U., Reina, C., 1998. Scaling EM (expectation-maximization) Clustering to Large Databases. Microsoft Research, pp. 0–25.
Brewer, C.K., Winne, J.C., Redmond, R.L., Opitz, D.W., Mangrich, M.V., 2005. Classifying and mapping wildfire severity. Photogrammetric Eng. Remote Sens. 71 (11), 1311–1320.
Buckland, M.K., 2019. What is a megafire? Defining the Social and Physical Dimensions of Extreme US Wildfires (1988-2014). University of Colorado at Boulder.
Cardil, A., Eastaugh, C.S., Molina, D., 2015. Extreme temperature conditions and wildland fires in Spain. Theor. Appl. Climatol. 122 (1), 219–228.
Cardil, A., et al., 2019. How does drought impact burned area in Mediterranean vegetation communities? Sci. Total Environ. 693, 133603.
Cattau, M.E., Wessman, C., Mahood, A., Balch, J.K., 2020. Anthropogenic and lightning-started fires are becoming larger and more frequent over a longer season length in the USA. Glob. Ecol. Biogeogr. 29 (4), 668–681.
Champeaux, J.L., Masson, V., Chauvin, F., 2005. ECOCLIMAP: a global database of land surface parameters at 1 km resolution. Meteorol. Appl.: J. Forecast. Practical Appl. Train. Tech. Modell. 12 (1), 29–32.
Clarke, H., Gibson, R., Cirulis, B., Bradstock, R.A., Penman, T.D., 2019. Developing and testing models of the drivers of anthropogenic and lightning-caused wildfire ignitions in south-eastern Australia. J. Environ. Manage. 235, 34–41.
Coen, J.L., Stavros, E.N., Fites-Kaufman, J.A., 2018. Deconstructing the King megafire. Ecol. Appl. 28 (6), 1565–1580.
Collins, B.M., Omi, P.N., Chapman, P.L., 2006. Regional relationships between climate and wildfire-burned area in the Interior West, USA. Canadian J. Forest Res. 36 (3), 699–709.
Dadap, N.C., Cobb, A.R., Hoyt, A.M., Harvey, C.F., Konings, A.G., 2019. Satellite soil moisture observations predict burned area in Southeast Asian peatlands. Environ. Res. Lett. 14 (9), 094014.
Dai, A., Trenberth, K.E., Qian, T., 2004. A global dataset of palmer drought severity index for 1870–2002: relationship with soil moisture and effects of surface warming. J. Hydrometeorol. 5 (6), 1117–1130.
de Dios, V.R., et al., 2022. Convergence in critical fuel moisture and fire weather thresholds associated with fire activity in the pyroregions of Mediterranean Europe. Sci. Total Environ. 806, 151462.
Dempster, A.P., Laird, N.M., Rubin, D.B., 1977. Maximum likelihood from incomplete data via the EM algorithm. J. R. Stat. Soc.: Ser. B (Methodol.) 39 (1), 1–22.
Dennison, P.E., Brewer, S.C., Arnold, J.D., Moritz, M.A., 2014. Large wildfire trends in the western United States, 1984-2011. Geophys. Res. Lett. 41 (8), 2928–2933.
Filliben, J.J., 1975. The probability plot correlation coefficient test for normality. Technometrics. 17 (1), 111–117.
Flannigan, et al., 2016. Fuel moisture sensitivity to temperature and precipitation: climate change implications. Clim. Change 134 (1), 59–71.
Flatley, W.T., Lafon, C.W., Grissino-Mayer, H.D., 2011. Climatic and topographic controls on patterns of fire in the southern and central Appalachian Mountains, USA. Landsc. Ecol. 26 (2), 195–209.

Fraley, C., Raftery, A.E., 2002. Model-based clustering, discriminant analysis, and density estimation. J. Am. Stat. Assoc. 97 (458), 611–631.
Fraley, C., Raftery, A.E., Murphy, T.B., Scrucca, L., 2012. Technical report.
Fujihara, Y., Tanaka, K., Watanabe, T., Nagano, T., Kojiri, T., 2008. Assessing the impacts of climate change on the water resources of the Seyhan River Basin in Turkey: use of dynamically downscaled data for hydrologic simulations. J. Hydrol. 353 (1–2), 33–48.
Fulé, P.Z., et al., 2003. Mixed-severity fire regime in a high-elevation forest of Grand Canyon, Arizona, USA. Landsc. Ecol. 18 (5), 465–486.
Geary, W.L., et al., 2022. Responding to the biodiversity impacts of a megafire: a case study from south-eastern Australia's Black Summer. Diver. Distribut. 28 (3), 463–478.
Greenwood, J.A., Landwehr, J.M., Matalas, N.C., Wallis, J.R., 1979. Probability weighted moments: definition and relation to parameters of several distributions expressable in inverse form. Water Resour. Res. 15 (5), 1049–1054.
Guttman, N.B., Hosking, J., Wallis, J.R., 1993. Regional precipitation quantile values for the continental United States computed from L-moments. J. Clim. 6 (12), 2326–2340.
Hao, Z., Hao, F., Singh, V.P., Zhang, X., 2018. Changes in the severity of compound drought and hot extremes over global land areas. Environ. Res. Lett. 13 (12), 124022.
Harma, K., Morrison, P., 2003. Analysis of Vegetation Mortality and Prior Landscape condition, 2002 Biscuit Fire Complex. Pacific Biodiversity Institute, Winthrop, WA.
Hayes, M., Svoboda, M., Wall, N., Widhalm, M., 2011. The Lincoln declaration on drought indices: universal meteorological drought index recommended. Bull. Am. Meteorol. Soc. 92 (4), 485–488.
Hersbach, H., et al., 2018. ERA5 hourly data on single levels from 1979 to present. Copernicus Climate Change Service (C3S) Climate Data Store (CDS), p. 10.
Higuera, P.E., Abatzoglou, J.T., 2021. Record-setting climate enabled the extraordinary 2020 fire season in the western United States. Glob. Chang. Biol. 27 (1).
Holden, Z.A., et al., 2018. Decreasing fire season precipitation increased recent western US forest wildfire activity. Proc. Natl. Acad. Sci. u S. a 115 (36), E8349–E8357.
Hoover, K., Hanson, L.A., 2021. Wildfire statistics. Congression. Res. Serv. 2.
Hosking, J.R., 1990. L-moments: analysis and estimation of distributions using linear combinations of order statistics. J. R. Stat. Soc.: Series B (Methodol.) 52 (1), 105–124.
Hosking, J.R.M. and Wallis, J.R., 1997. Regional frequency analysis.
Hurteau, M.D., Bradford, J.B., Fulé, P.Z., Taylor, A.H., Martin, K.L., 2014. Climate change, fire management, and ecological services in the southwestern US. For. Ecol. Manage. 327, 280–289.
Jia, S., Kim, S.H., Nghiem, S.V., Doherty, P., Kafatos, M.C., 2020. Patterns of population displacement during mega-fires in California detected using Facebook Disaster Maps. Environ. Res. Lett. 15 (7).
Jones, et al., 2021. Megafire causes persistent loss of an old-forest species. Anim. Conserv. 24 (6), 925–936.
Keeley, J.E., Baer-Keeley, M., Fotheringham, C., 2005. Alien plant dynamics following fire in Mediterranean-climate California shrublands. Ecol. Appl. 15 (6), 2109–2125.
Keeley, J.E., Safford, H., Fotheringham, C., Franklin, J., Moritz, M., 2009. The 2007 southern California wildfires: lessons in complexity. J. For. 107 (6), 287–296.
Keeley, J.E., Syphard, A.D., 2017. Different historical fire–climate patterns in California. Int. J. Wildland. Fire 26 (4), 253–268.
Kendall, M.G., 1948. Rank correlation methods.
Keyantash, J., Dracup, J.A., 2002. The quantification of drought: an evaluation of drought indices. Bull. Am. Meteorol. Soc. 83 (8), 1167–1180.
Kotsuki, S., Takenaka, H., Tanaka, K., Higuchi, A., Miyoshi, T., 2015. 1-km-resolution land surface analysis over Japan: impact of satellite-derived solar radiation. Hydrol. Res. Lett. 9 (1), 14–19.
Kotsuki, S., Tanaka, K., 2013a. Impacts of mid-rainy season rainfall on runoff into the Chao Phraya River, Thailand. J. Disaster Res. 8 (3), 397–405.
Kotsuki, S., Tanaka, K., 2013b. Uncertainties of precipitation products and their impacts on runoff estimates through hydrological land surface simulation in Southeast Asia. Hydrol. Res. Lett. 7 (4), 79–84.
Le Breton, T.D., et al., 2022. Megafire-induced interval squeeze threatens vegetation at landscape scales. Front. Ecol. Environ.
Littell, J.S., Peterson, D.L., Riley, K.L., Liu, Y., Luce, C.H., 2016. A review of the relationships between drought and forest fire in the United States. Glob. Chang. Biol. 22 (7), 2353–2369.
Liu, Y., Liu, B., Yang, X., Bai, W., Wang, J., 2015. Relationships between drought disasters and crop production during ENSO episodes across the North China Plain. Reg. Environ. Change 15 (8), 1689–1701.
Loehman, R.A., Reinhardt, E., Riley, K.L., 2014. Wildland fire emissions, carbon, and climate: seeing the forest and the trees–A cross-scale assessment of wildfire and carbon dynamics in fire-prone, forested ecosystems. For. Ecol. Manage. 317, 9–19.
Loveland, T.R., et al., 2000. Development of a global land cover characteristics database and IGBP DISCover from 1 km AVHRR data. Int. J. Remote Sens. 21 (6–7), 1303–1330.
MacQueen, J., 1967. Some methods for classification and analysis of multivariate observations. In: Proceedings of the fifth Berkeley symposium on mathematical statistics and probability. Oakland, CA, USA, pp. 281–297.
Malamud, B.D., Millington, J.D., Perry, G.L., 2005. Characterizing wildfire regimes in the United States. Proc. Natl. Acad. Sci. 102 (13), 4694–4699.
Mann, H.B., 1945. Nonparametric tests against trend. Econometrica: J. Econom. Soc. 245–259.
Mansoor, S., et al., 2022. Elevation in wildfire frequencies with respect to the climate change. J. Environ. Manage. 301, 113769.
Margolis, E.Q., Swetnam, T.W., 2013. Historical fire–climate relationships of upper elevation fire regimes in the south-western United States. Int. J. Wildland. Fire 22 (5), 588–598.
McMahon, G., et al., 2001. Developing a spatial framework of common ecological regions for the conterminous United States. Environ. Manage. 28 (3), 293–316.
Moody, J.A., Shakesby, R.A., Robichaud, P.R., Cannon, S.H., Martin, D.A., 2013. Current research issues related to post-wildfire runoff and erosion processes. Earth. Sci. Rev. 122, 10–37.
Moreira, F., Catry, F.X., Rego, F., Bacao, F., 2010. Size-dependent pattern of wildfire ignitions in Portugal: when do ignitions turn into big fires? Landsc. Ecol. 25 (9), 1405–1417.
Myhre, G., et al., 2019. Frequency of extreme precipitation increases extensively with event rareness under global warming. Sci. Rep. 9 (1), 16063.
Nagy, R.C., Fusco, E., Bradley, B., Abatzoglou, J.T., Balch, J., 2018. Human-related ignitions increase the number of large wildfires across US ecoregions. Fire 1 (1), 4.
Navarro, K.M., et al., 2021. Wildland firefighter exposure to smoke and COVID-19: a new risk on the fire line. Sci. Total Environ. 760, 144296.
Nocedal, J., Wright, S.J., 1999. Numerical Optimization. Springer.
Omernik, J.M., 1987. Ecoregions of the conterminous United States. Annal. Assoc. Am. Geographers 77 (1), 118–125.
Omernik, J.M., 2004. Perspectives on the nature and definition of ecological regions. Environ. Manage. 34 (1), S27–S38.
Omernik, J.M., Griffith, G.E., 2014. Ecoregions of the conterminous United States: evolution of a hierarchical spatial framework. Environ. Manage 54 (6), 1249–1266.
Oswalt, S.N., Smith, W.B., Miles, P.D., Pugh, S.A., 2019. Forest Resources of the United States, 2017: A Technical Document Supporting the Forest Service 2020 RPA Assessment. Gen. Tech. Rep. WO-97, 97. US Department of Agriculture, Forest Service, Washington Office., Washington, DC.
Özbayoğlu, A.M., Bozer, R., 2012. Estimation of the burned area in forest fires using computational intelligence techniques. Procedia Comput. Sci. 12, 282–287.
Palmer, W.C., 1965. Meteorological Drought, 30. US Department of Commerce, Weather Bureau.
Parks, S.A., Abatzoglou, J.T., 2020. Warmer and drier fire seasons contribute to increases in area burned at high severity in Western US forests from 1985 to 2017. Geophys. Res. Lett. 47 (22).
Parks, S.A., Holsinger, L.M., Miller, C., Parisien, M.A., 2018. Analog-based fire regime and vegetation shifts in mountainous regions of the western US. Ecography 41 (6), 910–921.
Pliscoff, P., Folchi, M., Aliste, E., Cea, D., Simonetti, J.A., 2020. Chile mega-fire 2017: an analysis of social representation of forest plantation territory. Appl. Geogr. 119, 102226.
Povak, N.A., Kane, V.R., Collins, B.M., Lydersen, J.M., Kane, J.T., 2020. Multi-scaled drivers of severity patterns vary across land ownerships for the 2013 Rim Fire, California. Landsc. Ecol. 35 (2), 293–318.
Riley, K.L., Abatzoglou, J.T., Grenfell, I.C., Klene, A.E., Heinsch, F.A., 2013. The relationship of large fire occurrence with drought and fire danger indices in the western USA, 1984–2008: the role of temporal scale. Int. J. Wildland. Fire 22 (7), 894–909.
Robichaud, P.R., 2000. Fire effects on infiltration rates after prescribed fire in Northern Rocky Mountain forests, USA. J. Hydrol. 231, 220–229.
Rodrigues, M., Gelabert, P.J., Ameztegui, A., Coll, L., Vega-García, C., 2021. Has COVID-19 halted winter-spring wildfires in the Mediterranean? Insights for wildfire science under a pandemic context. Sci. Total Environ. 765, 142793.
Scrucca, L., Fop, M., Murphy, T.B., Raftery, A.E., 2016. mclust 5: clustering, classification and density estimation using Gaussian finite mixture models. R J 8 (1), 289.
Sellers, P., et al., 1996. A revised land surface parameterization (SiB2) for atmospheric GCMs. Part I: model formulation. J. Clim. 9 (4), 676–705.
Serrano, A., Mateos, V., Garcia, J., 1999. Trend analysis of monthly precipitation over the Iberian Peninsula for the period 1921–1995. Phys. Chem. Earth Part B: Hydrol. Oceans Atmosphere 24 (1–2), 85–90.
Shabbir, A.H., et al., 2020. Predicting the influence of climate on grassland area burned in Xilingol, China with dynamic simulations of autoregressive distributed lag models. PLoS ONE 15 (4), e0229894.
Shen, L., Zhao, C., Yang, X., Yang, Y., Zhou, P., 2022. Observed slump of sea land breeze in Brisbane under the effect of aerosols from remote transport during 2019 Australian mega fire events. Atmos. Chem. Phys. 22 (1), 419–439.
Shi, K., Touge, Y., Kazama, S., 2022. Defining homogeneous drought zones based on soil moisture across Japan and teleconnections with large-scale climate signals. J. Appl. Meteorol. Climatol. 61 (1), 43–60.
Short, K.C., 2021. Spatial wildfire occurrence data for the United States, 1992-2018 [FPA_FOD_20210617].
Singh, V., Guo, H., Yu, F., 1993. Parameter estimation for 3-parameter log-logistic distribution (LLD3) by Pome. Stochastic Hydrol. Hydraulic. 7 (3), 163–177.
Stedinger, J.R., 1993. Frequency analysis of extreme events. Handbook of Hydrology.
Steel, Z.L., Safford, H.D., Viers, J.H., 2015. The fire frequency-severity relationship and the legacy of fire suppression in California forests. Ecosphere 6 (1).
Sturtevant, B.R., et al., 2009. Studying fire mitigation strategies in multi-ownership landscapes: balancing the management of fire-dependent ecosystems and fire risk. Ecosystems. 12, 445–461.
Swain, D.L., 2021. A shorter, sharper rainy season amplifies California wildfire risk. Geophys. Res. Lett. 48 (5), e2021GL092843.
Syphard, A.D., Radeloff, V.C., Hawbaker, T.J., Stewart, S.I., 2009. Conservation threats due to human-caused increases in fire frequency in Mediterranean-climate ecosystems. Conservat. Biol. 23 (3), 758–769.
Tanaka, K., 2005. Development of the new land surface scheme SiBUC commonly applicable to basin water management and numerical weather prediction model.

Tentoglou, T., Burmistrova, J., Hestir, E., 2021. Burn severity and albedo analysis concerning the mendocino complex fire. In: 2021 IEEE International Geoscience and Remote Sensing Symposium IGARSS, pp. 6496–6499.
Thackeray, C.W., Hall, A., Norris, J., Chen, D., 2022. Constraining the increased frequency of global precipitation extremes under warming. Nat. Clim. Chang. 12 (5), 441–448.
Trucchia, A., Meschi, G., Fiorucci, P., Gollini, A., Negro, D., 2022. Defining wildfire susceptibility maps in italy for understanding seasonal wildfire regimes at the national level. Fire 5 (1), 30.
USFS, 2015. The Rising Cost of Fire Operations: Effects on the Forest Service's Non-Fire Work. United States Department Agriculture Forest Service, Washington, DC, USA.
Van Mantgem, P.J., Falk, D.A., Williams, E.C., Das, A.J., Stephenson, N.L., 2020. The influence of pre-fire growth patterns on post-fire tree mortality for common conifers in western US parks. Int. J. Wildland. Fire 29 (6), 513–518.
van Wagtendonk, J.W., Moore, P.E., Yee, J.L., Lutz, J.A., 2020. The distribution of woody species in relation to climate and fire in Yosemite National Park, California, USA. Fire Ecol. 16 (1), 1–23.
Vehtari, A., Gelman, A., Gabry, J., 2017. Practical Bayesian model evaluation using leave-one-out cross-validation and WAIC. Stat. Comput. 27 (5), 1413–1432.
Vicente-Serrano, S.M., Beguería, S., López-Moreno, J.I., 2010. A multiscalar drought index sensitive to global warming: the standardized precipitation evapotranspiration index. J. Clim. 23 (7), 1696–1718.
Vieira, D., Fernández, C., Vega, J., Keizer, J., 2015. Does soil burn severity affect the post-fire runoff and interrill erosion response? A review based on meta-analysis of field rainfall simulation data. J. Hydrol. 523, 452–464.
Wang, Xiaoxiao, Di, Z., Li, M., Yao, Y., 2021. Satellite-Derived Variation in Burned Area in China from 2001 to 2018 and Its Response to Climatic Factors. Remote Sens. (Basel) 13 (7), 1287.
Wang, W., Zhu, Y., Xu, R., Liu, J., 2015. Drought severity change in China during 1961–2012 indicated by SPI and SPEI. Natural Hazards 75 (3), 2437–2451.
Ward Jr, J.H., 1963. Hierarchical grouping to optimize an objective function. J. Am. Stat. Assoc. 58 (301), 236–244.
Watanabe, S., Opper, M., 2010. Asymptotic equivalence of Bayes cross validation and widely applicable information criterion in singular learning theory. J. Mach. Learn. Res. 11 (12).
Wei, F., et al., 2020. Nonlinear dynamics of fires in Africa over recent decades controlled by precipitation. Glob. Chang. Biol. 26 (8), 4495–4505.
Wells, N., Goddard, S., Hayes, M.J., 2004. A self-calibrating Palmer drought severity index. J. Clim. 17 (12), 2335–2351.
Xu, K., Yang, D., Xu, X., Lei, H., 2015. Copula based drought frequency analysis considering the spatio-temporal variability in Southwest China. J. Hydrol. 527, 630–640.
Yaloveha, V., Hlavcheva, D., Podorozhniak, A., Kuchuk, H., 2019. Fire hazard research of forest areas based on the use of convolutional and capsule neural networks. In: 2019 IEEE 2nd Ukraine Conference on Electrical and Computer Engineering (UKRCON). IEEE, pp. 828–832.
Yang, J., et al., 2018. Comprehensive drought characteristics analysis based on a nonlinear multivariate drought index. J. Hydrol. 557, 651–667.
Ye, L., Hanson, L.S., Ding, P., Wang, D., Vogel, R.M., 2018. The probability distribution of daily precipitation at the point and catchment scales in the United States. Hydrol. Earth. Syst. Sci. 22 (12), 6519–6531.
Yelenik, S., Perakis, S., Hibbs, D., 2013. Regional constraints to biological nitrogen fixation in post-fire forest communities. Ecology 94 (3), 739–750.
Yue, S., Wang, C.Y., 2002. Applicability of prewhitening to eliminate the influence of serial correlation on the Mann-Kendall test. Water Resour. Res. 38 (6), 4-1–4-7.
Zhai, J., et al., 2010. Spatial variation and trends in PDSI and SPI indices and their relation to streamflow in 10 large regions of China. J. Clim. 23 (3), 649–663.
Zhang, L., Lau, W., Tao, W., Li, Z., 2020. Large wildfires in the Western United States exacerbated by tropospheric drying linked to a multi-decadal trend in the expansion of the hadley circulation. Geophys. Res. Lett. 47 (16).